Cloud Patterns, Waves and Convection in the Venus Atmosphere

MICHAEL J. S. BELTON AND GERALD R. SMITH

Kitt Peak National Observatory,[1] Tucson, Ariz. 85726

GERALD SCHUBERT AND ANTHONY D. DEL GENIO

Department of Geophysics and Space Physics, University of California, Los Angeles 90024

(Manuscript received 20 November 1975, in revised form 16 March 1976)

ABSTRACT

We provide morphological and kinematic descriptions of the UV markings seen in the Mariner 10 imagery of Venus: the dark horizontal Y, bow-like waves, circumequatorial belts, subsolar disturbance, spiral streaks and bands, polar ring and polar region. The dark horizontal Y is interpreted as a westward-propagating planetary wave with zonal wavenumber 1 and period ~4.2 days; it may be the superposition of a Rossby-Haurwitz wave dominant at mid-latitudes and a Kelvin wave dominant in equatorial regions. Bow-like waves may be true bow waves formed by the interaction of the rapid zonal flow with internal gravity waves of lower horizontal phase speeds generated by the subsolar disturbance. Circumequatorial belts are interpreted as internal gravity waves with horizontal wavelength ~500 km and zonal extent ~5000 km. They are essentially parallel to latitude circles and propagate southward at about 20 m s^{-1}. Cellular features in the subsolar region undoubtedly imply convection there. The identification of both bright- and dark-rimmed cells, with horizontal scales of about 200 and 500 km, respectively, implies a 15 km deep convective layer, based on an analogy with mesoscale convection in the terrestrial maritime atmosphere. The dark areas of the cells may be regions of downwelling. Variability in the location and intensity of the polar ring may be caused by a zonally propagating disturbance, perhaps related to the planetary wave producing the Y in lower latitudes. Circulation patterns and other atmospheric processes in the polar region may be rather different from elsewhere on the planet; only in the polar region are UV markings also visible in the orange.

1. Introduction

Two striking properties of Mariner 10 UV images of the upper Venus atmosphere (Murray *et al.*, 1974), and also of much lower resolution, ground-based UV pictures of the atmosphere, are their rough global-scale symmetry about the equator and the rapid ~4 day retrograde rotation of the brightness variations, corresponding to equatorial velocities of ~100 m s^{-1}. Do the motions of these UV features represent a bulk motion of the atmosphere or a wave propagation phenomenon (Young, 1975a)? It seems likely that both a bulk atmospheric rotation and propagating planetary-scale waves are revealed in the movement of UV contrasts, as the following discussion will show.

Venera measurements (Marov *et al.*, 1973; Ainsworth and Herman, 1975) and Earth-based spectroscopic observations (Traub and Carleton, 1975) leave little doubt that the dominant mode of circulation of at least the equatorial lower stratosphere and upper troposphere is a rotation from east to west with zonal wind speeds of ~100 m s^{-1}. Suomi (1974) has hypothesized that the motions of small-scale markings in the UV pictures represent the actual atmospheric winds, a view we adopt here. Accordingly, he has tracked such features and reported a meridional profile of the zonal wind with speeds of ~100 m s^{-1} in low and mid-latitudes.

Large-scale UV brightness variations, however, do not necessarily move with the actual bulk velocity of the atmosphere. In fact, on the basis of time-lapse pictures constructed from the Mariner 10 TV sequence, Belton *et al.* (1976) have proposed that the dominant dark horizontal Y pattern (cf. Boyer and Guérin, 1969; Scott and Reese, 1972; Beebe, 1972; Dollfus, 1975) and the modulation in position and intensity of the bright polar ring (Murray *et al.*, 1974) are the manifestations of planetary-scale propagating waves. The proposition is based on the differences in the motions of large- and small-scale UV contrasts; the globally coherent Y pattern repeats itself approximately in 4.2 days implying a uniform rotation of the pattern, whereas the small-scale UV markings, presumably reflecting the actual atmospheric winds, are moving too fast at mid-latitudes for the upper atmosphere to be uniformly rotating. Our ability to infer both actual atmospheric winds and propagating planetary waves from motions of UV contrasts depends crucially on having imagery of

[1] Kitt Peak National Observatory is operated by the Association of Universities for Research in Astronomy, Inc., under contract with the National Science Foundation.

sufficient resolution to identify features of both global, regional and local scale and to track the movement of these features, noting any dependence of the motion on scale size. In the Mariner 10 pictures we have imagery of the requisite resolution and coverage.

It is ironic that the movement of large-scale UV contrasts visible from Earth originally suggested the possibility of a rapid, bulk retrograde rotation of the entire upper atmosphere, while the Mariner 10 interpretation associates traveling waves with these large-scale contrasts and bulk motions with small-scale features not visible from Earth. With respect to an observer in space, planetary waves would be seen to propagate at the sum of the bulk velocity of the atmosphere and the local phase velocity of the wave. Thus, if relevant planetary waves move slowly compared with the actual atmospheric rotation of Venus, they can also reveal the approximate underlying circulation. This is apparently the situation for the motions of the large-scale UV contrasts seen in the ground-based imagery and the inferences on actual upper atmospheric circulation drawn therefrom.

In view of the above, the present work has as its underlying philosophy the possibility that the morphology and temporal development of markings in the Mariner 10 pictures may contain much useful information on the dynamical processes which maintain the observed atmospheric motions. For example, the vertical redistribution of zonal momentum by planetary-scale waves, stimulated in some way by the passage of the Sun, could be responsible for the rapid rotation of the upper Venus atmosphere (Leovy, 1973; Fels and Lindzen, 1974; Ramanathan and Cess, 1975) and such waves might be *seen* in the Mariner 10 pictures. Similar processes are thought to take place in the Earth's tropical stratosphere (Holton, 1972; Wallace, 1973). One westward-propagating mode can in fact be "seen" in the motions of cloud patterns in Earth-satellite pictures (Chang, 1970). It is also possible that processes which *limit* the magnitude of the rapid rotation could involve wave generation and large-scale instabilities and be visible in the pictures.

The main purpose of this paper is, therefore, to provide a detailed and, wherever possible, quantitative description of major phenomena seen in the 8 days of Mariner 10 observation and to identify any obvious relationships between them. In this sense much of the material presented here supersedes the preliminary information given by Murray *et al.* (1974). We consider all the major phenomena identified in the preliminary report irrespective of the possible importance of wave processes to their generation or maintenance. These phenomena include the dark horizontal Y, circumequatorial belts, bow-like waves, subsolar disturbance, mid-latitude spiral streaks, polar ring and polar region.

In addition, we present our interpretations of some of these phenomena in terms of physical processes that are familiar in the Earth's atmosphere. Of necessity these interpretations contain many conjectural assumptions and it is possible that our reliance on terrestrial experience could turn out to be dangerously misleading; these interpretations are therefore offered with great caution. Noticeably absent is any form of discussion or new insight into the chemical nature of the light and dark markings. Thus our basic interpretive assumption is that there is a direct relationship between the relative presence of light and dark material and the local thermodynamic state of some level high in the Venus atmosphere.

2. The data set

All 3400 useful frames that were taken during the 8 days of the Mariner 10 Venus encounter were examined in the course of this study. This large amount of material was batch processed and conveniently made available to the authors on 70 mm film and high-quality microfiche. Individual pictures that were selected for further study were specially processed at the Jet Propulsion Laboratory and made available either as paper hardcopy, as film prints, or in digital form on tape. Measurements were made either directly on the paper hardcopy or with the help of the Interactive Picture Processing System located at Kitt Peak National Observatory. This latter device is a computer-TV monitor combination that allows real-time manipulation and measurement of digital picture data.

The precision of the measurements of linear scales, angles and velocities is not the highest that the Mariner 10 pictures are capable of yielding for, unlike the study of winds (Suomi, 1974), we have taken only modest precautions in assuring the geometric fidelity of the pictures. Nevertheless, the uncertainties quoted in our measurements seem adequate for the main purposes of this study, and in light of this, the great cost savings realized by minimizing the emphasis on geometric precision seems to be justified.

Measurements of the motion and orientation of the circumequatorial belts and the bow-like waves were made in the following manner. The basic reference was the center of the planet as defined by the limb. Limb points were measured at the 12% of full scale intensity level. The coordinates of the center pixel[2] and the radius were determined by a least-squares solution. On the average 15 points defined the limb and the rms deviation from the best center was normally less than a pixel. From a sample of 30 pictures measured in this way we find a mean range-radius product of $(5.92 \pm 0.12) \times 10^8$ km-pixels, which, with the ground calibration of 10.39 μrad per pixel,[3] gives an effective plane-

[2] Each television picture is constructed of an array of 700×832 elements. Individual picture elements are called "pixels".

[3] In the Mariner 10 system the pixels in the original pictures are not square. In discussing distance in a picture or its absolute calibration we always work in terms of the dimension of a pixel in the line sweep (sample) direction.

tary radius of 6150±120 km. At the mean range of 2.5×10^6 km for this sequence of pictures the uncertainty of 120 km translates into about 5 pixels. In computing velocities we have assumed an effective planetary radius of 6120 km, an average value for the distance of the UV atmospheric features from the planet's center (see the interpretation section for a discussion of the level in the atmosphere seen in UV).

In order to compare pictures taken at different times and to examine the geometry of the circumequatorial belts it was necessary to perform rotations of the pictures to a standard coordinate system. The information required to do this was obtained from precise ephemerides provided by the Mariner 10 project and the assumption that the horizontal line direction in the pictures points toward the Sun. Prelaunch calibration ensured that this is the case to better than 0.1° and the spacecraft limit cycle should not add more than a ±0.25° uncertainty to this. The standard coordinate system assumed in this study rotates in a retrograde sense with a period of 243.0 days and has the planet's orbit about the Sun as its fundamental plane. In describing directions in the pictures we have used the International Astronomical Union convention for defining the points of the compass. Because of Venus' retrograde rotation this means north is in the direction opposite to the direction of the angular momentum vector, as defined by the right-hand rule.

The spacecraft's flight data system (FDS) provided a unique tag for each frame (FDS number). In discussing the sequence of events that take place in the pictures we shall often refer to this number since it provides the reader with a convenient link to the basic data set. During the flight this number was incremented once every 42 s. Venus encounter occurred at FDS 57800 and it may be helpful to remember that an FDS increment of 10000 (~4.9 days) is roughly equivalent to the apparent rotation period of the upper atmosphere.

Descriptions giving details of the flyby trajectory, picture taking sequence, cameras and picture characteristics have been published previously by Dunne (1974) and by Murray *et al.* (1974).

3. Global properties of the UV markings

Following Venus encounter, Mariner 10 viewed Venus for a period of 8 days at a low, roughly constant phase angle. The phase angle changed from 29° at the completion of the first full disk mosaic to roughly 23° at the termination of the sequence. Thus throughout most of the period roughly two-thirds of the illuminated part of the planet was available for study with the subsolar point near the center of the image. The geometric center of the image was about 20° upwind (east) of the subsolar point and at latitude −17°; it changed very slowly through the 8-day sequence. The viewing conditions were therefore best for observations of the Southern Hemisphere. Foreshortening diminished any real chance of making observations further north than about 50° latitude.

In a mosaic of pictures taken about one day after encounter (Fig. 1a) the planet is characterized by a dark equatorial belt roughly 25° wide in latitude which stretches from limb to terminator. As time progresses the dark belt is seen to terminate and by FDS 62693 (2.4 days after encounter) bright material has moved in from the east and covered the equatorial zone from the subsolar point to the terminator (Fig. 1b). At the same time darker markings are making their appearance at higher latitudes on the equatorial side of the polar ring (Fig. 1b). The equatorial region remains bright until FDS 65787 (~1.5 days later) when a dark horizontal Y appears at the equatorial terminator (Fig. 1c). The planet is seen to regain its original distribution of brightness (but not in all of its specific details) by FDS 68835, 5.4 days after encounter (Fig. 1d). The sequence continues to unfold as before with the appearance of darker markings at high latitudes near FDS 71300 (~4.2 days later than this kind of situation was first seen). At the cessation of the TV coverage (FDS 74340) a dark horizontal Y is again seen to appear at the equator. This is roughly 4.2 days after its first appearance.

These progressive changes of brightness in the large-scale features and the phase relationships of markings at different latitudes can also be seen in the longitude vs time sequence of Fig. 2. Because of the long lifetime of large-scale features, the same effects can also be seen in the latitude vs time composite pictures described by Belton *et al.* (1976). The repetition in the large-scale pattern of markings after ~4.2 days and the progressive change in phase of the brightness distribution with latitude can be clearly seen in these latter pictures.

In summary: The large-scale brightness distribution between ±50° latitude, seen over roughly two "apparent" 4.2-day rotations of the pattern, is roughly symmetric about the equator and periodic with a dominant zonal wavenumber of 1. This periodicity is maintained away from the equator but is less well defined in mid-latitudes. The phase of the brightness distribution appears to advance westward with increasing latitude. At the latitude of the polar ring, about ±50°, the phase has increased by approximately 130°. The overall impression given by the brightness distribution is of a single, dark, horizontal Y encircling the planet (Belton *et al.*, 1976).

Underlying the changes in brightness distribution outlined above we have noticed two other characteristics which stand out and which may be significant.

1) The basic features of the high-frequency spatial detail near the equator are different depending on whether the region is covered by light or dark material.

2) Transitory phenomena such as the propagation of the circumequatorial belts and the appearance of the

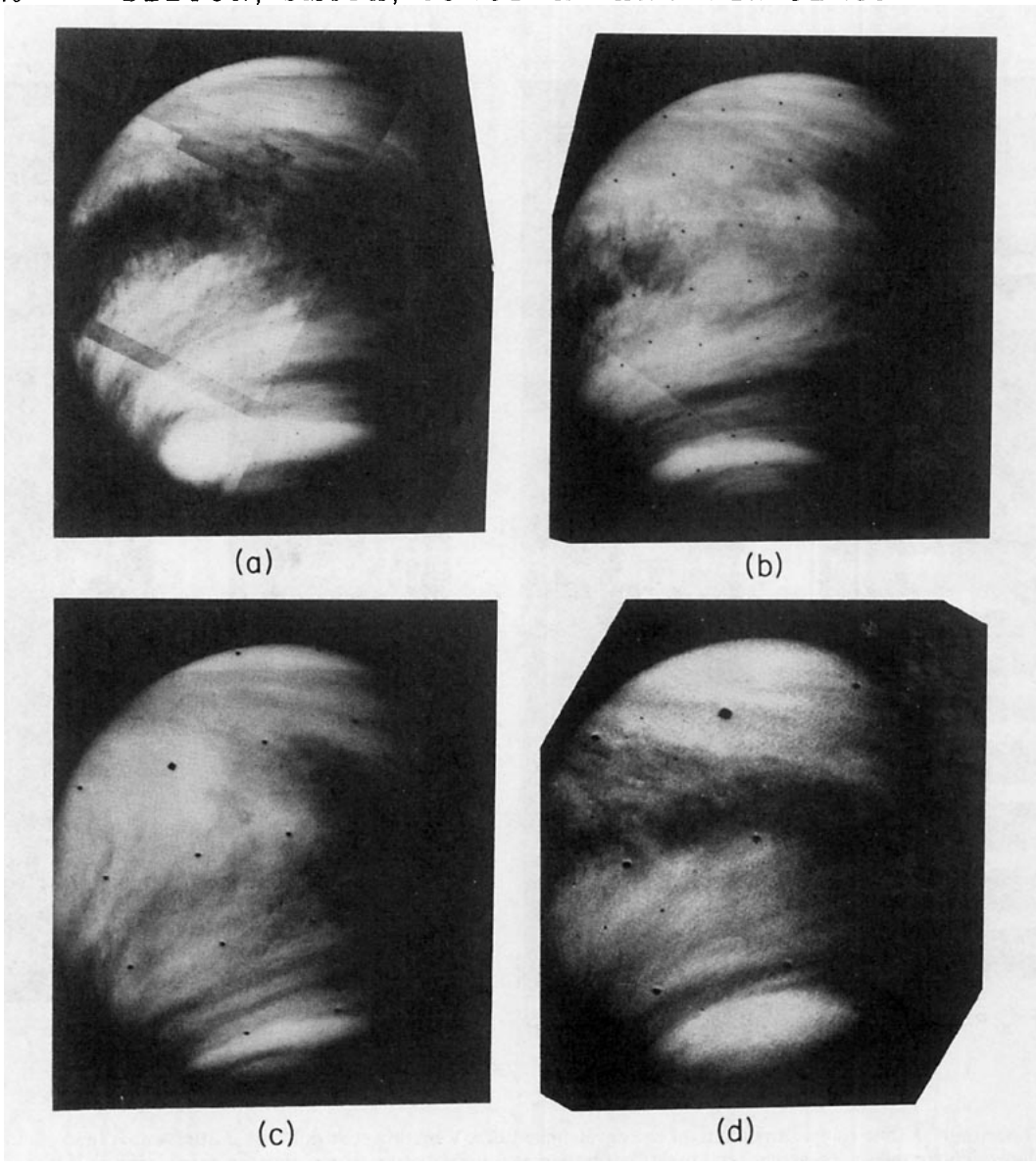

FIG. 1. Development of the UV markings with time. The tones of these pictures and mosaics reflect the actual brightness distribution on the planet in the UV [$\lambda \approx 3550$ Å; see Murray *et al.* (1974)]. The contrast has been strongly enhanced, but the picture data are unsmoothed and unfiltered. Representative times and FDS numbers are:

(a) Encounter+1 day (FDS 59883)
(b) Encounter+2.4 days (FDS 62693)
(c) Encounter+3.9 days (FDS 65787)
(d) Encounter+5.36 days (FDS 68835).

bow-like waves are only seen in the equatorial region while bright material is present.

The observations of these and all other special phenomena are described in detail in the following section.

4. Description of special phenomena

Murray *et al.* (1974) have identified and briefly described the following seven specific phenomena or characteristic regions in the Mariner 10 pictures: the dark horizontal Y, circumequatorial belts, bow-like waves, subsolar disturbance, mid-latitude spiral streaks, polar ring and polar region. We have found no new features to add to this list but the following material should provide a much more comprehensive description of each of them. The Y pattern has already been discussed in the previous section and in Belton *et al.* (1976).

a. Circumequatorial belts

The first clear sign of a circumequatorial belt (CEB) was found in FDS 61946, roughly coincident with the

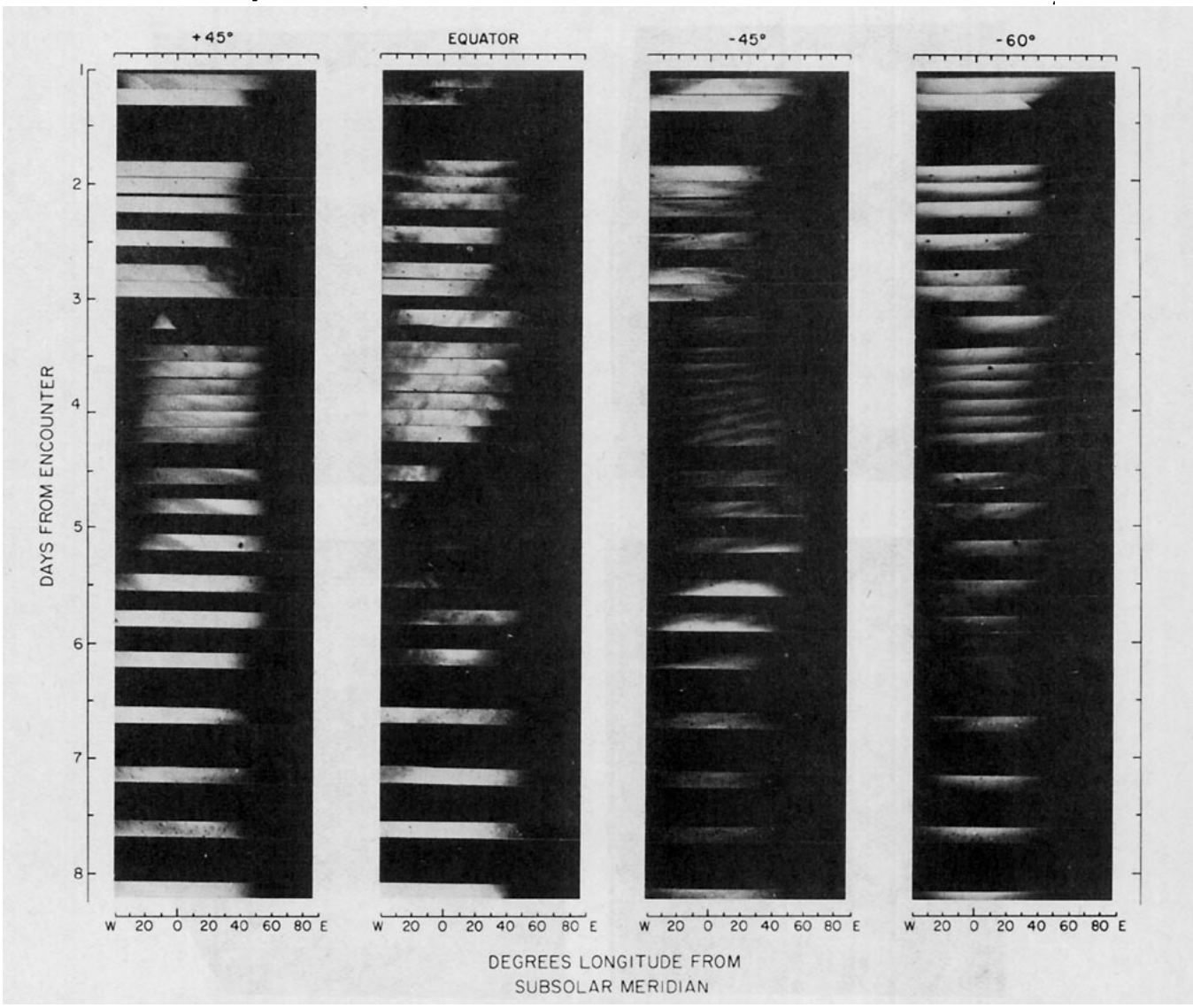

FIG. 2. Longitude vs time composite picture of the development of UV markings at different latitudes on Venus. As in Fig. 1, the tones of these pictures reflect the actual brightness distribution along zonal strips at an effective wavelength of 3550 Å. The gaps in the pictures are primarily a reflection of gaps in the Mariner 10 picture taking sequence and are therefore unavoidable. Nevertheless, the roughly "periodic" changes of brightness associated with large-scale features (Belton *et al.*, 1976) and the directions and rates of motion of smaller scale features can easily be seen. Note the phase of the pattern at higher latitudes compared to that at the equator. The picture corresponding to −60° latitude is characteristic of the region poleward of the south polar ring.

passage of bright material over the subsolar meridian. The belt appeared near +8° latitude and was very sharp (2–3 pixels) and continuous over its ~2000 km length. By FDS 62078, ~1.5 h later, two other CEB's had appeared in the Southern Hemisphere (−7° and −12° latitude). All of these features propagated toward the south. The display reached its peak near FDS 63000, when as many as five CEB's were seen simultaneously. The phenomenon was essentially over by FDS 65000, 1½ days after its onset, although there were some very weak indications of the phenomenon as late as FDS 66067.

Measurements were made on 20 pictures to determine the geometry, dimensions and propagation velocity of the belts. Fig. 3 shows the position of the belts on the subsolar meridian as a function of FDS number and also their frequency of occurrence in the pictures as a function of latitude. Fig. 4 shows the spatial distribution of all the individual CEB measurements and Fig. 5 illustrates the relationship of a single CEB [(3) of Fig. 3] to the subsolar point as it propagates.

The CEB's have the following properties:

1) They are found only near the equator between latitudes ±20° [Fig. 3; see also, Fig. 8 in Belton *et al.*

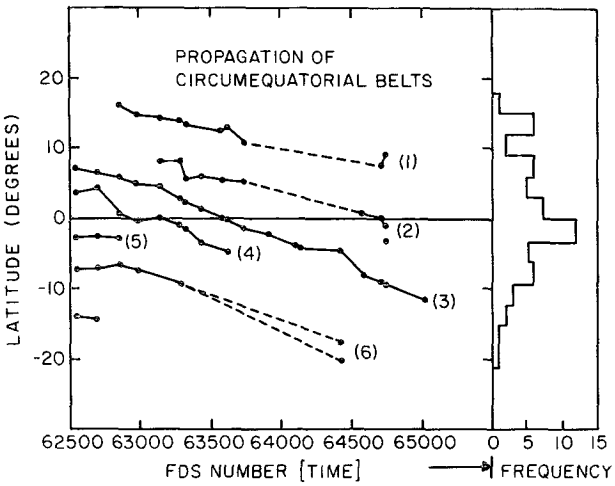

FIG. 3. Meridional propagation and distribution of circumequatorial belts. The ordinate is latitude. At the left of the figure the abscissa is the FDS number and, at the right, it is the observed frequency of occurrence of CEB's within 3° latitude intervals. The data points are taken from 20 selected Mariner 10 pictures and the latitudes are measured at the subsolar meridian. The lines joining the points are intended to show the progress of a single CEB; where this is uncertain a broken line is used. Each number identifies a particular CEB.

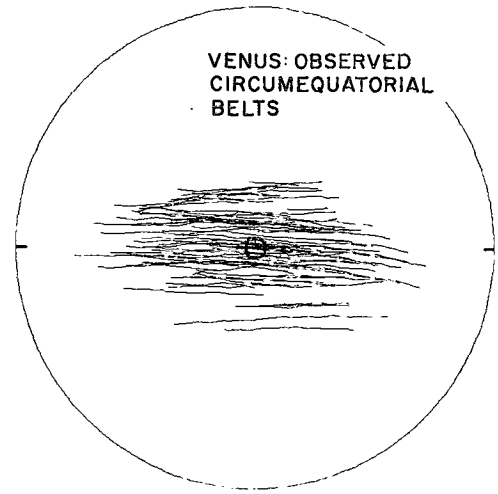

FIG. 4. Distribution of observed circumequatorial belts relative to the subsolar point. The belts are shown in orthographic projection centered on the subsolar point. Latitude circles are horizontal lines in this plot and the planetary disk is outlined by a circle. The data are from 20 Mariner 10 pictures.

(1976)] and they occur only near the subsolar point (Fig. 4).

2) When many belts are seen at a single time they appear to be evenly spaced. The separation is about 4°–5° of latitude or about 500 km (cf. Figs. 1b and 3).

3) They have variable length (~5000 km) and are roughly parallel to lines of latitude (Fig. 4). The angles that the circumequatorial belts make with lines of constant latitude are uncertain due to measurement errors by $\sim\pm 3°$.

4) With the exception of a single case the width of the belts is near or below the resolution limit ($\lesssim$50 km). In the single exception the belt was perhaps 150 km wide.

5) The individual belts appear in 1–2 h and propagate for 0.5–1.5 days.

6) They propagate only toward the south (Fig. 5) with relatively slow phase speeds. A least-squares linear fit to the data in the case of the belt marked (3) in Fig. 3 gives a meridional propagation velocity of about 3×10^{-6} rad s^{-1} or 20 m s^{-1} relative to the surface.

7) They do not appear to partake in the underlying 90–100 m s^{-1} zonal velocity, although there may be a tendency for individual belts to drift to the west at a much lower apparent rate (~40 m s^{-1} or less). In Fig. 5 we can see some suggestion of a small westward drift during the southward propagation of the belts.

b. Bow-like waves

The bow-like waves are first noticeable in the picture sequence near FDS 65000 (Fig. 6) when the display of CEB's is dying out. They become very prominent in the equatorial subsolar region by FDS 65343 [Fig. 7; also note the features marked (b) on FDS 65473 of Fig. 6] and maintain their visibility until they disappear from view over the limb. Fig. 6 shows the global aspect of the phenomenon while Fig. 7, which is a Mercator projection, illustrates the details which are described below. Fig. 2–4 and 11 in Belton *et al.* (1976) show different views of the growth of the waves.

In their preliminary results Murray *et al.* (1974) noted that these features propagate through (or over) the subsolar disturbance at roughly 80% of the average

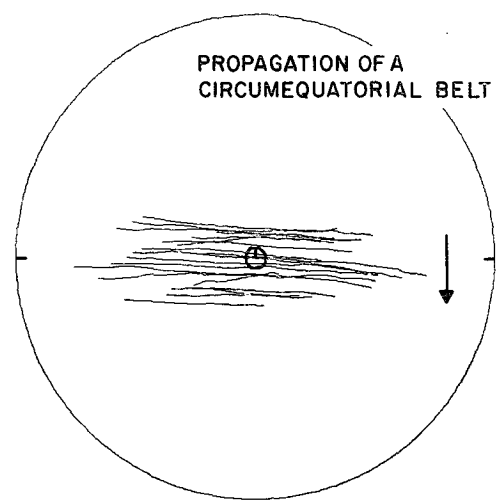

FIG. 5. Propagation of a single circumequatorial belt [(3) in Fig. 3]. The geometry of the plot is the same as in Fig. 4. The direction of motion is indicated by the arrow.

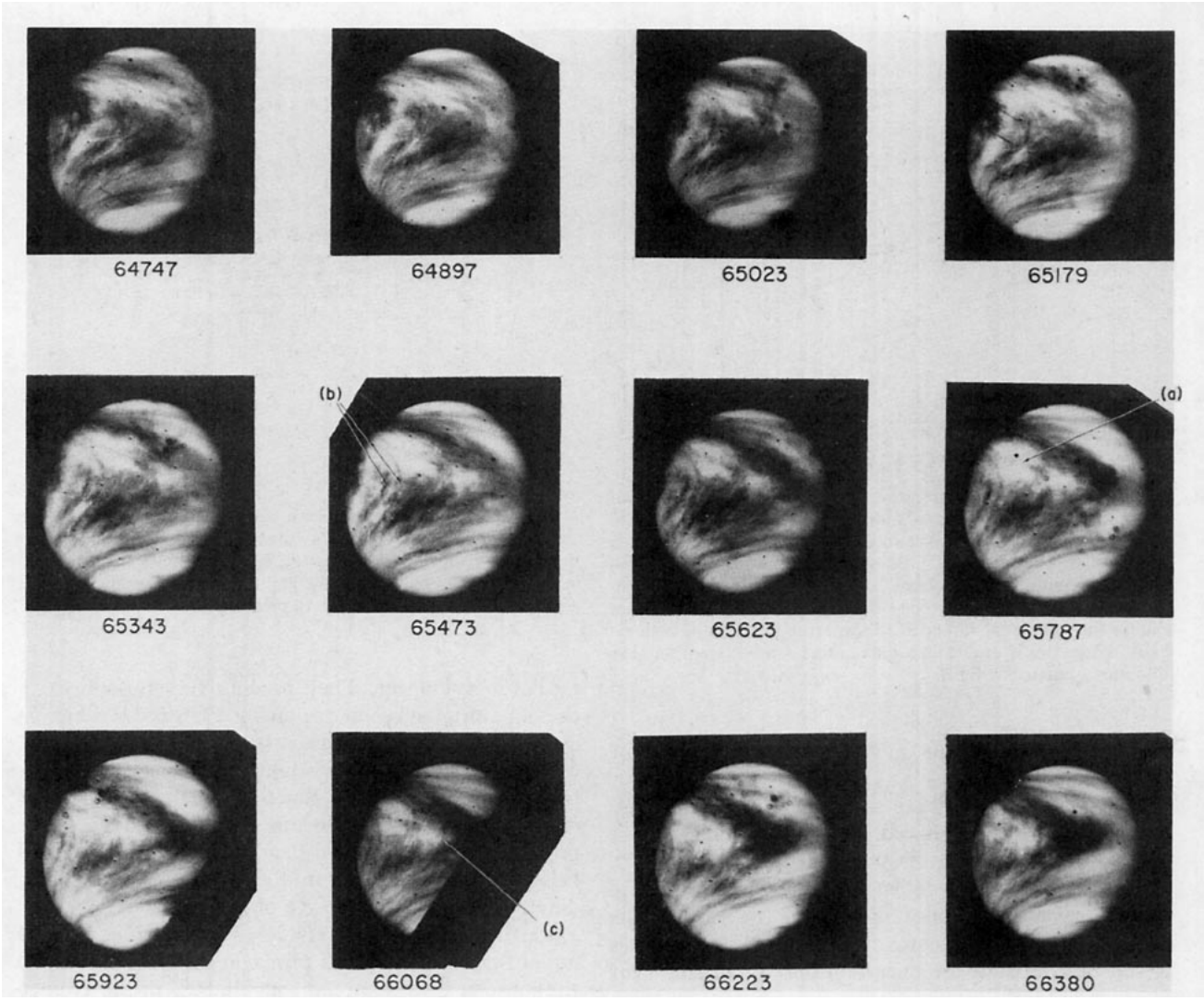

FIG. 6. Development of the bow-like wave phenomenon. The symbols (a), (b), (c) represent, respectively, the precursor, the bow-like waves, and another feature similar to a bow-like wave forming in the vertex of the dark horizontal Y.

rotation speed. However, the measurements reported below indicate that once formed, they move with the general zonal motion of the small-scale UV markings (Suomi, 1974). The bow-like waves have the following characteristics:

1) They form with their vertices on the equator about 5° upwind of the subsolar meridian at about the time when the circumequatorial belt phenomenon is seen to be finally fading out.

2) The wave furthest to the west forms first, followed (within 4 h) by a second wave about 8° upstream. Each wave appears as far as we can tell in its entirety and we find no obvious evidence in the pictures that a propagating disturbance forms the waves. The waves extend to roughly $\pm 30°$ latitude (Fig. 7).

3) There is a third feature, which we call the precursor [(a) in FDS 65787 of Fig. 6], which may also be associated with the phenomenon. This precursor has essentially the same geometry as the dark horizontal Y which follows in the progression of markings, and occurs almost exactly halfway between the vertex of the Y and the vertices of the two most prominent bow-like waves.

4) The equatorial zonal velocity of the bow-like waves was found to be 93 ± 5 m s^{-1} (Fig. 8) in agreement with measurements of the general wind field by Suomi (1974). The change in shape of a bow-like wave with time is illustrated in Fig. 9. The wave maintains its shape with time in southerly latitudes where the measurements are most reliable, implying no change in its angular velocity with latitude.

5) There is an indication of an additional bow-like wave forming in the vertex of the dark horizontal Y as its passes through the subsolar region [feature (c) on FDS 66068 in Fig. 6].

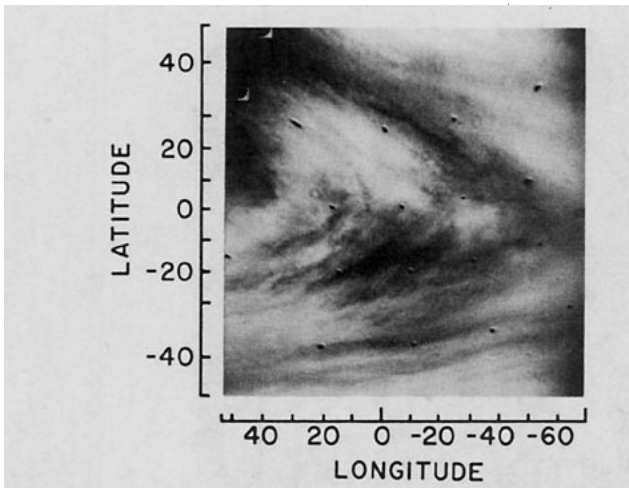

FIG. 7. Mercator projection (FDS 65343) of the bow-like wave phenomenon. This picture shows the geometry and scale of the waves and their relation to the dark horizontal Y whose vertex can be seen at −50° longitude. Longitude is measured westward relative to the subsolar meridian.

c. *The subsolar disturbance, spiral streaks, and features in the equatorial region*

Throughout the Mariner 10 sequence there is a clear distinction between the morphological character of the UV markings near and downwind of the subsolar point, in mid-latitudes, and upwind of the subsolar point (Murray *et al.*, 1974). Nevertheless, despite the clarity of this distinction it is difficult to make *precise* statements about the properties of these three basic regions because of the continually changing scene at high spatial

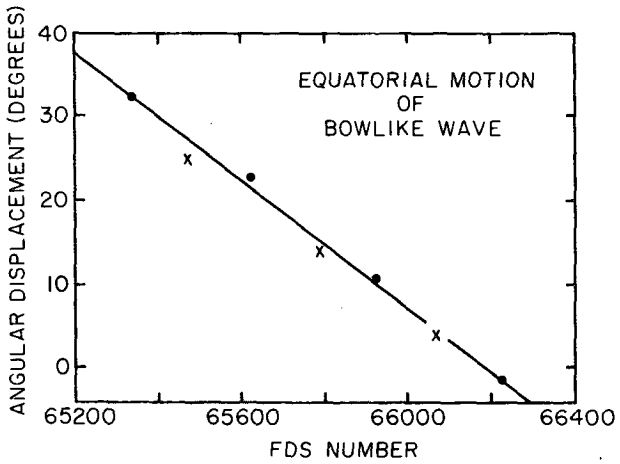

FIG. 8. Angular displacement of the vertex of the second (eastward) bow-like wave with respect to the subsolar meridian as a function of time (FDS number). The slope of the least-squares straight line fit gives a velocity of 93±5 m s^{-1}. The filled circles and crosses represent measurements made at widely separated times on two different sets of pictures [(FDS 65343, 65623, 65923, 66223) and (FDS 65473, 65787, 66067)], respectively. We have distinguished these two sets of points to illustrate the influence of systematic errors incurred in making the measurements.

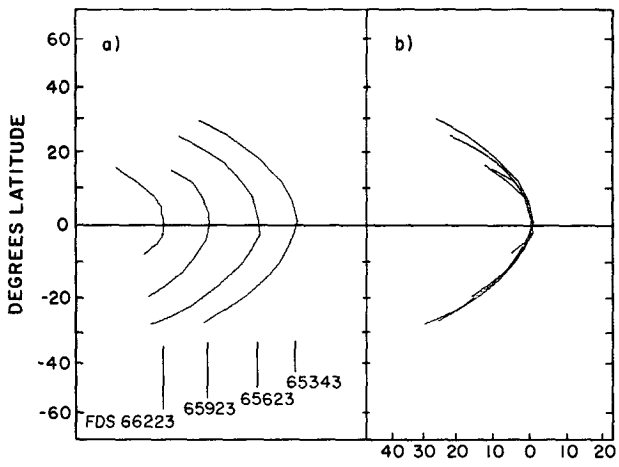

FIG. 9. Development of a bow-like wave with time. The shape of a bow-like wave at four different times is illustrated in (a). In each case the projection of the bow-like wave on a sphere is seen from a point directly above the vertex of the wave. The arms of the wave appear shorter as time progresses because of the motion of the wave toward the planetary limb in the original frame of reference. The symmetry of these features about the equator is clearly seen. In (b) these four observations of the bow-like waves are plotted so that their vertices coincide. There is little evidence for a change in shape with time. The scale of the abscissa of part (a) is identical to that of (b) with the exception that the zero point should be displaced to the vertex of each individual bow-like wave.

frequencies. What follows, therefore, is more in the nature of generalized impressions and may need substantial modification when applied to a particular picture.

d. *The subsolar disturbance (SSD)*

Near and immediately downwind of the subsolar point, extending 10°–20° north and south, the small-scale (~100 km) UV markings are generally quite chaotic, although there is often a tendency to group into cellular features. This is particularly noticeable along the northern and southern boundaries of the region where in the early part of the Mariner 10 sequence there is a transition between light and dark (Fig. 10). There is little organization of the markings near the subsolar meridian, but a tendency for the markings to organize into north-south alignments can be seen further downwind (~50°) [Fig. 10 and FDS 58018 in Fig. 11]. As this organization becomes more obvious the cellular nature of the markings disappears.

We have not been able to perform a detailed study of the cellular features including, for example, the distribution of scale size and lifetime, primarily because of the difficulty of identifying the same cell in successive mosaics. This problem has at its root an adverse coupling of the following effects: the nature of the flyby trajectory, limitations to the pointing stability (limit

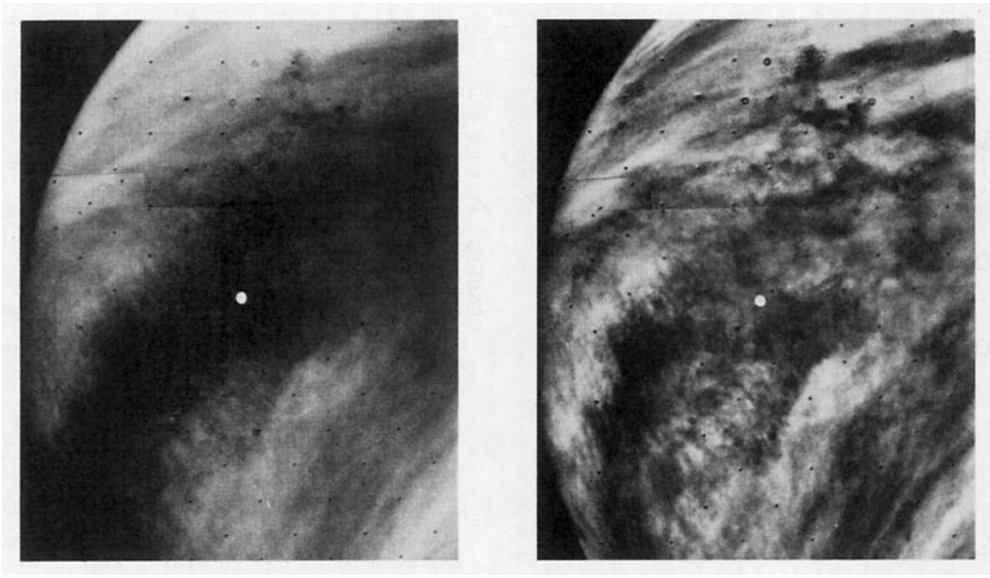

FIG. 10. Mosaic of frames (FDS 59861, 59881, 59882) illustrating the subsolar disturbance. The version of the picture on the left is contrast-enhanced but it reflects the original brightness distribution. The picture on the right has been spatially filtered to emphasize the finestructure. The white dot shows the location of the subsolar point. Note the presence of cellular features in the region where the transition from light to dark takes place and the appearance of a pattern with north-south alignment in the markings that cross the equatorial region some distance downwind of the subsolar point. This pattern is illustrated at higher resolution in Fig. 11.

cycle) of the spacecraft, and the restricted rate at which pictures could be transmitted from the spacecraft. The first caused a rapid drop-off in spatial resolution as the sequence progressed, while the last, in the case of the Mariner 10 system, led to large time gaps in global coverage early in the sequence, exactly when spatial resolution was required. The limit cycle unfortunately caused the voids (gores) in the high-resolution mosaics to repeatedly occur in the vicinity of the SSD. Nevertheless we were able to determine the following facts.

1) There are at least two types of cellular features, bright-rimmed cells with darker centers (Fig. 12) and, on a larger scale, a system of structures which are bounded by a dark filamentary network (Fig. 13).

2) The filamentary network is difficult to discern, and has been positively identified only on a few frames taken 24 h after encounter when the spatial resolution was about 14 km. Several of the cells are distinctly polygonal and their linear scale is about 500 km. We have traced this network over an area of approximately 2×10^7 km^2 ($\sim$5% of the planet's surface area) in the vicinity of the subsolar point (Fig. 13).

3) The bright rimmed cells are more obvious. They are seen distinctly even as late in the sequence as FDS 68106 (resolution $\sim$80 km) and are most visible in the region of transition between light and dark material bordering the SSD. In the early part of the sequence the cells can be seen to persist near the northern border of the dark to light transition all the way to the limb. The linear scale of the cells is roughly 200 km. There is little evidence of these cells upwind of the subsolar meridian but they are quite visible 10° of longitude downwind. This may imply a growth time of 3 h or less. We have attempted to follow the development of prominent groups of these cells, but the time gaps of 2–4 h that exist in the sequence are too long to achieve repeated identification. Our impression is that the lifetime of these features cannot be more than a few hours.

The above phenomenon, while having its greatest visibility in light material, has only been detected when the equatorial region is itself dark. In the part of the sequence from FDS 63450 to FDS 67500, when the subsolar disturbance region is bright, no obvious organized cellular structure of the type discussed above is seen. It is possible that this loss of identification could be caused by a combination of increasingly lower spatial resolution and a lack of contrast in the cells with the background material, but it might also be due to the simple absence of the phenomenon.

e. Mid-latitude region and spiral streaks

The mid-latitude markings are characterized by a greater degree of spatial coordination than is the case for the subsolar region. Whether in light or dark areas the markings are arranged in streaks roughly parallel to one another. The highest resolution frames easily resolve the basic structure; it has cross-dimensions of

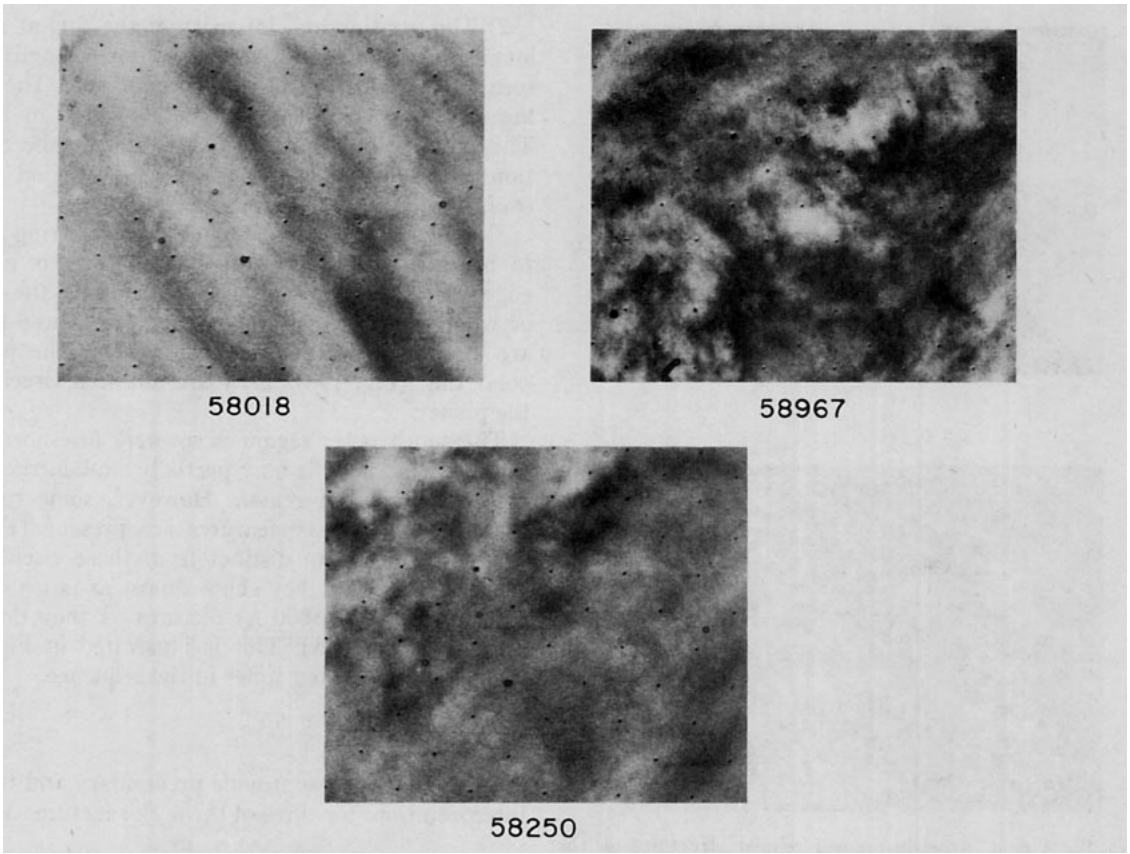

FIG. 11. The subsolar disturbance at higher resolution. FDS 58018 shows north-south alignments in the SSD at −13° latitude approximately 50° downwind of the subsolar point. FDS 58967 shows the chaotic nature of finestructure in the SSD at 8° latitude, 2° downwind of the subsolar point. FDS 58250 shows the state of the SSD at latitude +1°, about 15° upwind of the subsolar point. North is roughly toward the upper left-hand corner of these pictures which have been spatially filtered to emphasize finestructure.

~100 km and a length of ~1000 km (Fig. 14). Occasionally this basic pattern is perturbed by finer scale structure. For example, FDS 58156 in Fig. 14 shows the basic streak pattern in a dark region crossed by a much finer and essentially orthogonal pattern of streaks with a "wavelength" of about 20 km.

The small-scale streak morphology forms the basis of the spiral "streaks" discussed by Murray *et al.* (1974). In this paper we call these features spiral "bands" in order to distinguish them from the smaller scale markings of which they are composed. The bands, ~1000 km across and ~10000 km in length, consist of two ribbons of bright material in both hemispheres which spiral roughly halfway around the planet, extending from the equatorial region to ~50° latitude. The most prominent of these bands is seen in the Southern Hemisphere and it appears to be continuous across the equatorial region with a similar feature in the Northern Hemisphere (Fig. 15). This connection takes place when bright material covers the equatorial region (Fig. 15a). In this case the morphology of the spiral bands in the equatorial region is very similar to that of the bowlike waves. In Fig. 15b the equatorial region is dark and the spiral bands do not cross the equator.

The spiral bands are not in any sense true spirals and the development of the phenomenon is quite complex. The earliest mosaics contained two bright bands which were strongly inclined to lines of latitude. As the sequence progressed only the more prominent and southerly one remained in view and by FDS 61350 it was essentially parallel to lines of latitude (Fig. 15b). Later, the inclination of this band increased rapidly until, near FDS 62987, it extended into and across the equatorial region (Fig. 15a). The finestructure in the spiral bands also had a very distinct filamentary quality at this point which was not seen at other times (Fig. 14).

f. The equatorial region upwind of the subsolar point

Fig. 16 illustrates the character of the equatorial region upwind of the subsolar point, toward the morning terminator, when the region was covered by dark material. It shows diffuse streaks roughly aligned in an east-west direction, upon which is superimposed a

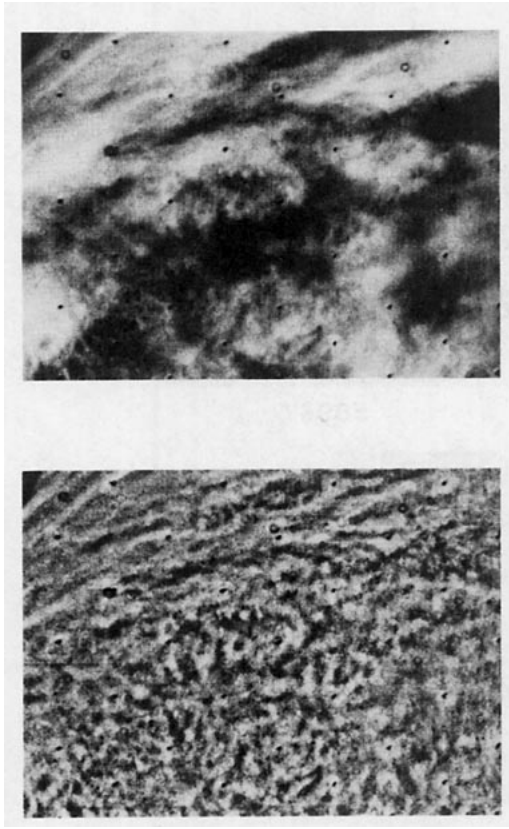

FIG. 12. A field of bright-rimmed cellular structures on the northern edge of the subsolar disturbance. The top picture is a contrast-enhanced version; the bottom picture has been spatially filtered in order to bring out the fine-scale structure.

faint indication of north-south alignments. The latitudinal separation of these features is about 160 km. When dark material is not present on the equator these features disappear and the finestructure is dominated by a somewhat broken field of markings upon which is superimposed the characteristic alignments associated with spiral bands and bow-like waves.

h. Polar ring and polar region

The southern polar ring was briefly described, on the basis of a very limited sample of pictures, by Murray *et al.* (1974) as the most distinctive and stable feature in the light markings. This description needs considerable modification in order to take into account the following observations:

1) The description of the feature as a "ring" is not entirely satisfactory. At times (Fig. 17) it is seen (FDS 66380) to cross latitude lines at a substantial angle (~20°), usually (but not always) in a northeast-southwest direction, while at other times it is essentially parallel to latitude circles (FDS 61650). In addition a "break" of the polar ring is evident in one of the high-resolution mosaics (Fig. 18).

2) The position and intensity of the ring at a given longitude with respect to the subsolar longitude are seen to be modulated as a function of time. The changing aspect of the polar ring is illustrated in Fig. 17. This modulation appears to be related to the modulation in the brightness of the equatorial region (Belton *et al.*, 1976).

3) While the body of the southern polar ring appears to be essentially devoid of finestructure its northern edge shows a wealth of detail, including the hooked or whorl structures shown in Fig. 19a. These features are also seen on the southern edge of the northern polar ring (Fig. 19b). They are not seen elsewhere on the planet.

The south polar region is severely foreshortened in the pictures and this may partially explain the lack of fine detail in the region. However, some relatively broad and contrasty features are present (Fig. 20). These markings are distinct from those elsewhere on the planet in that they show almost as much contrast in the orange (~5800 Å) pictures as they do in the ultraviolet (3550 Å). This is illustrated in Fig. 20 at two widely separated times in the sequence.

5. Interpretation

In this section we provide preliminary and tentative interpretations for three of the major features described

FIG. 13. Dark-edged cellular structures in the vicinity of the subsolar point. The top picture is a contrast enhanced version of FDS 59882. The lower part of the figure shows traces of the locations of the dark boundaries.

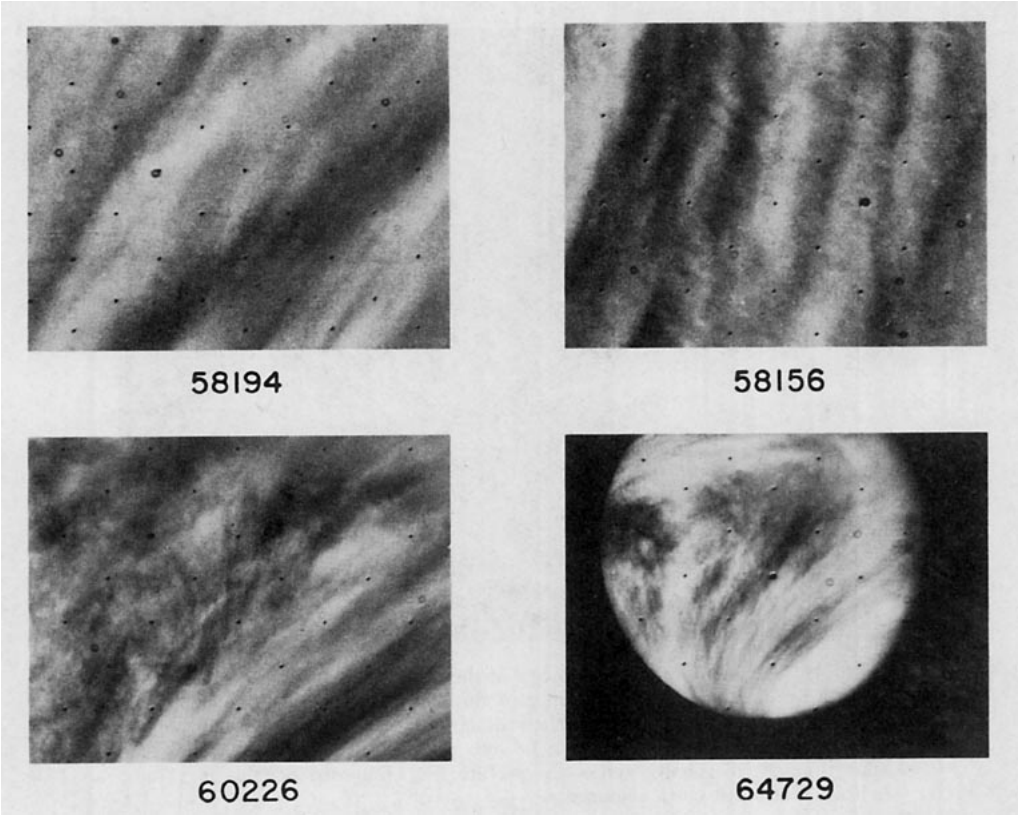

FIG. 14. Mid-latitude spiral band regions. FDS 58194 (latitude = −32°; ∼7° upwind of subsolar meridian) illustrates the basic streak morphology characteristic of these UV markings. FDS 58156 (latitude = −38°, ∼10° downwind of subsolar meridian) shows finestructure superimposed on the basic streak pattern. FDS 60226 (latitude = −26°, ∼13° upwind of subsolar meridian) is an example of the finestructure that develops in the spiral bands as they sweep up to the equator. FDS 64729 shows the same phenomenon as FDS 60226 but roughly half a rotation earlier when dark markings are present at the equator.

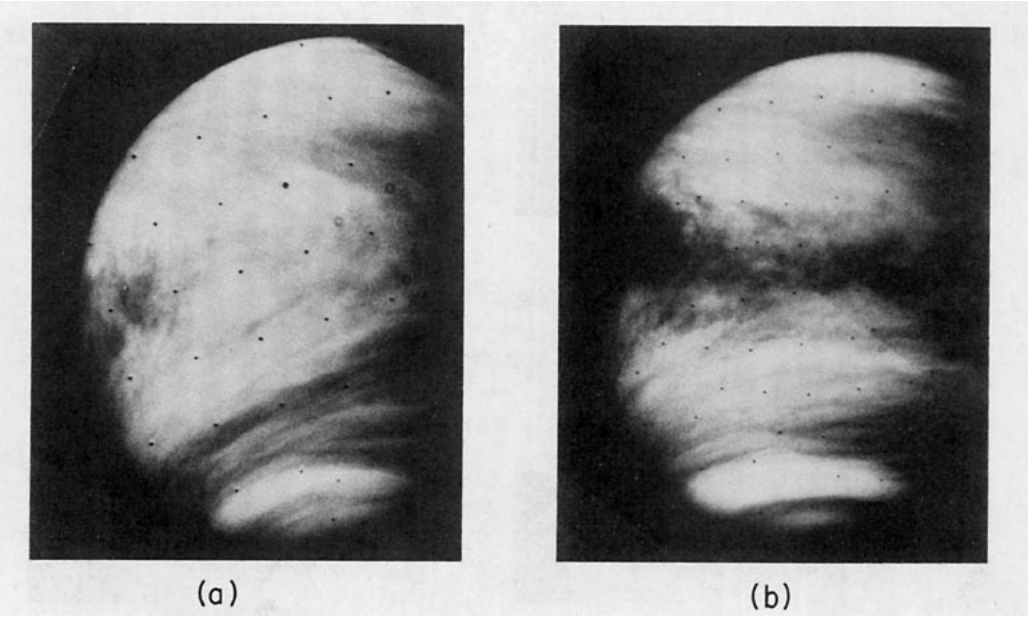

FIG. 15. Spiral bands: (a) FDS 62987 demonstrates the continuity of bright spiral bands across the equatorial region and their inclination to latitude circles. (b) FDS 61350 shows how at other times the bright spiral bands are roughly parallel to latitude lines. The dark band that appears to encircle the planet essentially follows the equator.

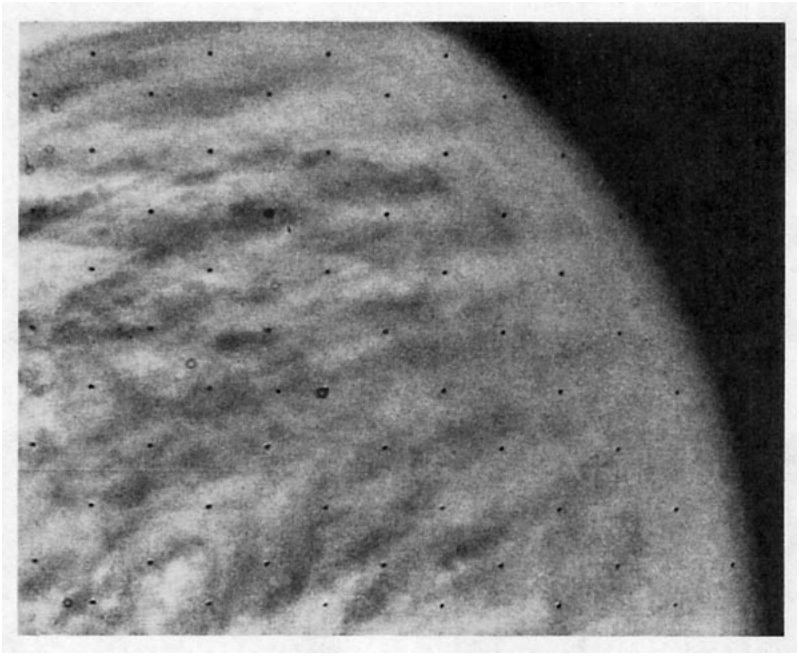

FIG. 16. The equatorial region upwind of the subsolar point when it was entirely covered by dark material. The center of this filtered picture (FDS 59888) is at −5.3° latitude and 59° upwind of the subsolar meridian. The morning terminator is on the right. Diffuse streaks can be seen parallel to the equator which runs approximately diagonally across the picture. Superimposed on this is a faint indication of north-south alignments.

previously, namely, the dark horizontal Y, the circum-equatorial belts, and the cellular structures of the subsolar disturbance. These features may be associated with planetary-scale waves, internal gravity waves and convection, respectively. We also offer a few more speculative comments regarding the nature of the bow-like waves.

In the terrestrial atmosphere, many different types of waves, some of which are important in the tropics and others in mid-latitudes, are known to exist; consequently, it is reasonable to seek an explanation of certain Venus UV brightness variations in similar wave propagation phenomena. On a global scale, Kelvin waves and mixed Rossby-gravity waves transport

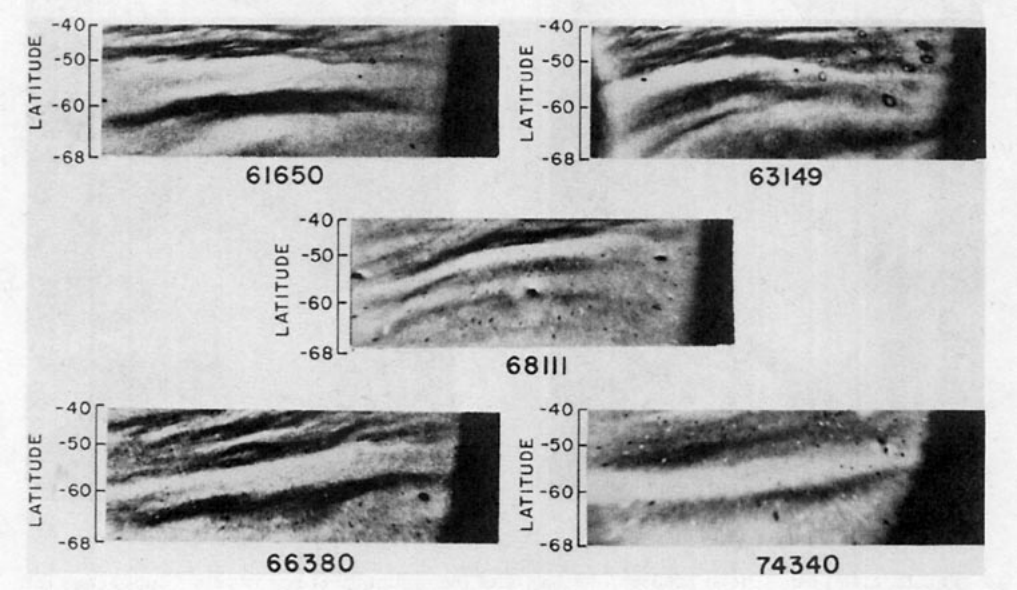

FIG. 17. This group of pictures of the south polar ring illustrates its variable geometry and brightness. A Mercator projection is used and the abscissa which stretches from limb to terminator (approximately 140°) is linear in longitude.

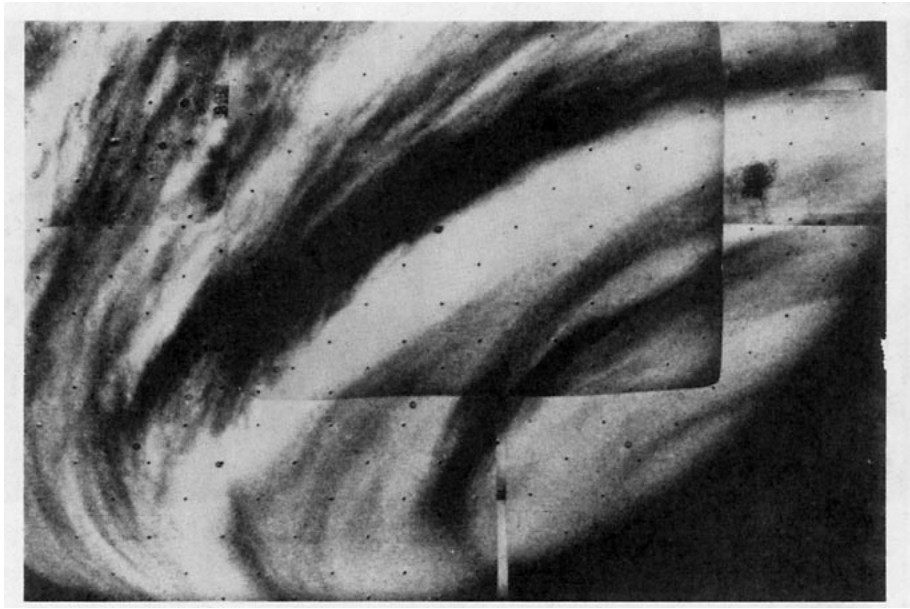

FIG. 18. A mosaic of frames (near FDS 59072) covering the region of the southern polar ring. The ring is apparently broken toward the southwest limb. This picture also provides one of the best views of markings in the polar region to the south of the ring and has been spatially filtered in order to emphasize small-scale features.

energy and momentum upward in the Earth's equatorial stratosphere (Wallace, 1973). Kelvin waves in the Earth's upper atmosphere are observed to be primarily of zonal wavenumber 1. Rossby waves are important disturbances in the Earth's upper atmosphere in mid-latitudes; we can cite, for example, the meandering of the polar front jet as a phenomenon associated with Rossby waves. Internal gravity waves of more limited scale are responsible for many phenomena in the terrestrial upper atmosphere, among which are mountain lee waves, wavelike variations in ionization, irregular variations in temperature and wind velocity, and, most notably, wavelike structures in noctilucent clouds (Hines, 1972).

Cloud patterns have been used to infer the existence and properties of propagating internal gravity waves in the Earth's atmosphere; propagation speeds and wavelengths are similar to those of the circumequatorial belts in the upper Venus atmosphere. Wavelike striations in photographs of terrestrial noctilucent clouds (Witt, 1962) have been interpreted as internal gravity waves at altitudes of about 80 km with horizontal

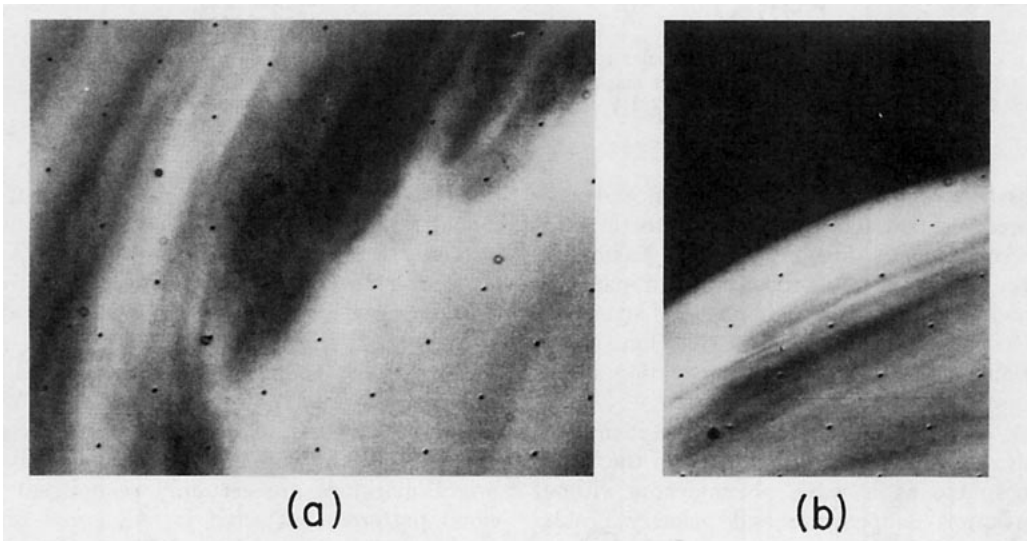

FIG. 19. Examples of hooked or whorl structures on the equatorial sides of the (a) southern and (b) northern polar rings.

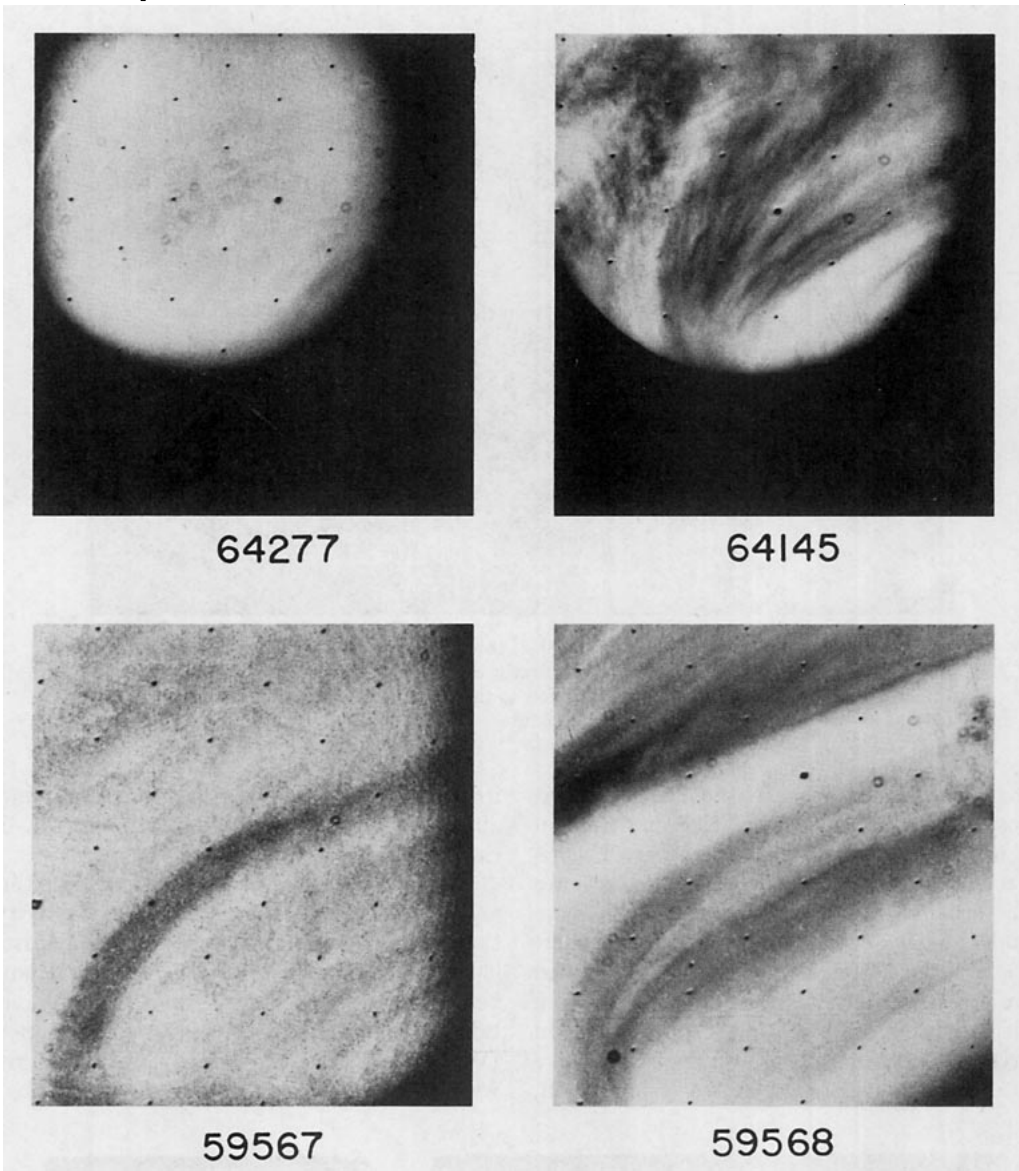

FIG. 20. Markings in the south polar region which show up strongly in orange pictures (5800 Å). No other region on the planet shows markings with as much contrast in the orange. FDS 64277 and 59567, orange; FDS 64145 and 59568, UV.

wavelengths between about 10 and 100 km and with speeds between 10 and 100 m s^{-1} relative to the local winds. Recent satellite imagery of the Earth has revealed the presence of horizontally propagating internal gravity waves in tropospheric cloud structures with wavelengths between 10 and 300 km (mean $\sim$100 km) and with characteristic propagation speeds about 40 m s^{-1} (Thomas *et al.*, 1975).

Of course, it is impossible to positively identify a particular feature in the UV observations of the Venus upper atmosphere as a wave phenomenon without detailed pressure, temperature and velocity profiles in the vertical and horizontal over a sufficiently long time. Instead of these, we have only limited observations of albedo variations. Even in our own atmosphere, the identification of cloud patterns and fluctuations as waves is a risky business, and many of the wave types which meteorologists have predicted from theory have been observed beyond any reasonable doubt only in the past 15 years.

Aside from the paucity of observations, we must surely regard any interpretation of the UV markings as tentative at best, because we are still uncertain as to what the bright and dark markings really are. The bright markings are certainly reminiscent of simple cloud patterns, but what is to be said of the dark markings? Are they regions of evaporation of the bright cloud material, i.e., clearings where we see to a greater

depth in the atmosphere? Or are they cloud patterns themselves, representing the condensation of some unknown ultraviolet absorber (Young, 1975b) at the same level as the bright markings? Until these questions are answered, we cannot hope to unravel the complex dynamics of the upper Venus atmosphere.

In view of the above comments, it is clear that we must make some basic interpretive assumptions. We assume that the UV contrasts are caused by a single physical phenomenon. The validity of this assumption may be limited to latitudes equatorward of the polar rings since in the polar region the markings also become obvious in the orange. We further assume that the nonuniform atmospheric rotation inferred by Suomi (1974) and the uniform rotation of the Y deduced by Belton *et al.* (1976) are correct.

Also fundamental to the interpretation of the UV contrasts is an estimate of the level in the atmosphere at which the UV phenomena are occurring. The markings are constrained to be between the 5 and 400 mb levels (~80–55 km) by direct observation at the upper boundary and by Rayleigh scattering limitations to UV visibility (Murray *et al.*, 1974). The most likely level to be representative of the UV markings is near the $\tau=1$ level in UV scattering as determined by polarization measurements in the UV. The global average level is ~50 mb or ~60 km (Hansen and Hovenier, 1974).

The 50 mb or 60 km level is the level at which, according to both Mariner 5 and Mariner 10 occultation experiments, there are distinct layered structures with characteristic vertical scale ~2 km. Also this level is essentially at the boundary of two regions of different vertical stability; above this level the atmosphere is very stable, while below it the atmospheric lapse rate, for about 15 km, is close to the dry adiabat. The region just below ~60 km may in fact be slightly unstable. This possibility is supported by observations of turbulent layers at 45 and 60 km (Woo, 1975) and by Lacis' (1975) calculations of the levels of maximum solar heating.

a. Dark horizontal Y

The observations of this paper and those of Belton *et al.* (1976) indicate that the large-scale pattern of UV markings referred to as the dark horizontal Y rotates with constant angular velocity. The associated period is ~4.2 days and the corresponding equatorial velocity is 103 ± 10 m s^{-1}. Thus at a latitude of 45° the zonal velocity of the large-scale UV pattern is only about 73 m s^{-1}, much smaller than the speed of the zonal winds at this latitude. A detailed computer analysis of small-scale features by Suomi (1974) gives zonal wind velocities of 92 m s^{-1} at the equator, increasing to 105 m s^{-1} at −45° latitude, and then decreasing to the pole, with rms uncertainties of about 5 m s^{-1} at the equator. Whether the wind velocity is actually constant with latitude or has a maximum at mid-latitudes, it is fairly certain that the atmosphere at these levels is not in a state of solid-body rotation as the large-scale UV features seem to be. If the small-scale markings are indeed tied to the atmospheric flow, the large-scale markings cannot be. In mid-latitudes, large-scale UV features are apparently propagating upstream (eastward) relative to the winds at a velocity of ~20–30 m s^{-1}. At the equator, the large-scale markings may be propagating westward relative to the mean flow at a velocity of ~5–15 m s^{-1}, or, due to the uncertainties in the measurements, they may be stationary relative to the bulk atmospheric flow.

We thus propose with Belton *et al.* (1976) that the dark horizontal Y is a wave phenomenon. Its apparent propagation at different speeds and in different directions at different latitudes seems to argue against an explanation in terms of any one single wave. This is supported by the detailed structure of the large-scale UV markings. The Y consists of an extremely dark, well-defined equatorial marking and a slightly less prominent dark marking in mid-latitudes which is advanced in longitude relative to the equatorial marking by ~130°. However, in the region between these two markings, in the neighborhood of 30° latitude, brightness variations are more subdued, although the "cloud patterns" at these latitudes appear to be tilted in such a way as to couple the equatorial and mid-latitude dark markings. Thus, the Y may be thought of as the visual addition of two features which maintain a relatively constant phase relationship to each other over a span of at least 4 days.

To determine the types of waves that may be responsible for the large-scale UV markings, we examine the solutions of Laplace's tidal equation on a sphere. We assume that the UV markings are cloud patterns formed, for example, in response to pressure fluctuations associated with the waves, and we seek wave patterns whose pressure perturbations have a spatial structure reminiscent of the Y.

Laplace's tidal equation is an eigenvalue equation governing fluid motions on a sphere. Its solution is governed by a dimensionless parameter

$$\epsilon=\frac{4\Omega^2a^2}{gh}, \tag{1}$$

where Ω is the rotation rate of the atmosphere, a the radius of the planet, g the gravitational acceleration, and h the depth of the undisturbed fluid. Usually, this equation is solved for the case of a thin, homogeneous, incompressible fluid in hydrostatic balance. In the case of a compressible, stratified fluid, an analogous form of Laplace's tidal equation for the latitudinal structure applies (Taylor, 1936); a vertical structure equation determines the dependence of the solutions on altitude. In this case h is not the depth

of the fluid, but rather an "equivalent depth" whose only physical significance is that the compressible, stratified fluid oscillates in a manner analogous to a homogeneous, incompressible fluid of depth h.

The equivalent depth is related to the frequency σ and longitudinal wavenumber s by the dispersion relation, and is calculated in one of two ways, depending on the problem being considered. For free oscillations, h depends on the basic state of the atmosphere and can be calculated from the vertical structure equation. Knowing h, the dispersion relation then tells us which pairs of σ, s are possible solutions on a sphere. For forced oscillations, we must specify σ, s from the character of the forcing (or the phase speed of the forced wave). The dispersion relation then gives us the appropriate value of h to use in computing ϵ, which in turn is then employed in Laplace's tidal equation to calculate the latitudinal structure of the mode.

The solutions of Laplace's tidal equation are of the form $e^{i(s\phi-\sigma t)}$ multiplied by functions of latitude and height. They are waves propagating in longitude ϕ with zonal speed σ $a\cos(\theta/s)$ (θ is latitude). The latitudinal solutions, consisting of series of Legendre functions, are known as "Hough functions," each mode being characterized by an order n. Longuet-Higgins (1968) presents plots of σ vs ϵ (equivalent to the dispersion relation) and graphs of the θ-dependences of the solutions for various values of n, s. For application to Venus, we base the value of the rotation rate Ω on the apparent 4-day period of the atmosphere's retrograde rotation. For simplicity, we study planetary waves in a uniformly rotating atmosphere, although the measurements just discussed indicate that Venus' upper atmosphere is not in uniform rotation.

We seek any combination of modes whose pressure fluctuations give a spatial pattern resembling the large-scale UV markings. For the purpose of illustration we first examine the free oscillation case. It is well known that the free oscillations of the atmosphere fall into two distinct classes; the oscillations of the first class (the gravity waves) which dominate in equatorial regions, and those of the second class (the Rossby-Haurwitz waves) which have their greatest amplitudes in mid-latitudes. Therefore, a combination of two of these waves, one from each class, might be appropriate.

Free Rossby-Haurwitz waves on Venus would travel eastward (due to Venus' retrograde rotation) with a phase speed of $\sim$20–25 m s^{-1}, which matches the upstream velocity of the Y inferred by Belton *et al.* (1976) at $-45°$ latitude. At the equator, free gravity waves would have phase velocities greater than 200 m s^{-1}, much larger than the observed speed of the Y relative to the zonal flow. However, a combination of two oppositely moving but otherwise similar gravity waves could form a standing wave pattern (first class oscillations may propagate eastward or westward, unlike the second class oscillations) relative to the atmospheric circulation and drift with it. Recall that this is one of the possible interpretations of the equatorial observations.

Since the Mariner 10 pictures show only one Y, which stretches around the entire planet, we select the wavenumber $s=1$. Because the pattern in mid-latitudes is shifted in longitude relative to the markings at the equator, we impose a phase shift on the Rossby-Haurwitz wave relative to the gravity wave. As an example of a possible meridional structure, we choose the lowest symmetric mode for both waves, that is, $n=1$ for the gravity wave and $n=2$ for the Rossby-Haurwitz wave. The Venusian temperature structure is complex, rendering the free oscillation problem very difficult. However, there are several types of thermal profiles which can be treated analytically and which are characterized by single values of the equivalent depth. Among these are an isothermal profile (based on the cloud-top temperature), an adiabatic profile, and a more general profile, $T(z)=a+bp(z)^{\kappa}$, where $\kappa=R/C_p$ and a, b are chosen to best fit the observed Venus temperature profile. For free oscillations on Venus, all of these profiles give values for ϵ of order 1. We present illustrative results for both $\epsilon=1$ and $\epsilon=10$ (approximately the correct value for Earth). The second class wave has greater amplitude and the first class wave is more confined to the equatorial region in the case $\epsilon=10$ as compared with $\epsilon=1$.

Fig. 21 shows surface elevation (pressure) contours which result from adding the two waves $Z_1^1(\theta)\cos\phi$ and $Z_1^2(\theta)\cos(\phi+90°)$ for $\epsilon=10$ (bottom of Fig. 21), and $Z_1^1(\theta)\cos\phi$ and $2Z_1^2(\theta)\cos(\phi+120°)$ for $\epsilon=1$ (top of Fig. 21). Here Z_s^n are normalized latitudinal solutions for the elevation of the free surface from equilibrium in the homogeneous incompressible problem (Longuet-Higgins, 1968). The parameter corresponding to Z_s^n in the more realistic compressible stratified problem is the pressure fluctuation, which would have the same structure. The patterns resemble observed Mariner 10 UV features in two ways. The contour lines are tilted between 0° and $\pm45°$ latitude in such a way as to reproduce the basic shape of the Y. If we imagine that the physical processes responsible for the formation of the Y, for example, condensation and evaporation, can occur only in regions of greatest upwelling and downwelling, then we might expect to see visual evidence of these processes only within the highest amplitude contours, for instance ±0.5. These contours are effectively confined to within $\pm50°$ latitude, as are the UV features in the Mariner 10 imagery.

We have shown that it is possible to simulate the Y on Venus by considering several of the free modes of oscillation of an equivalent model atmosphere with a simple temperature profile and uniform rotation; the same is true for forced oscillations. The Venus atmosphere is probably capable of a strong response to many types of thermal or dynamical forcing, because of its mass, relative proximity to the Sun, and relatively slow rotation rate (Schubert and Young, 1970). Many

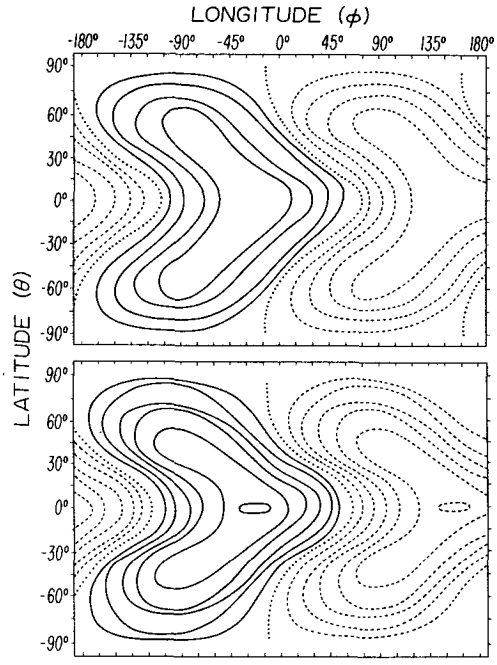

FIG. 21. Contours of surface elevation (pressure) for the free oscillation case obtained by combining a gravity wave with a Rossby-Haurwitz wave shifted westward in phase relative to the gravity wave. The lowest symmetric latitudinal mode for each wave ($n=1, 2$, respectively) is shown. The zonal wavenumber is 1. The latitudinal solutions are normalized so that the total energy over the sphere is a constant. The solid contours denote excess elevation, and the dashed ones denote elevation deficiencies. The dotted curves indicate no elevation change. Contour interval is 0.1.

Top: $Z_1^1(\theta)\cos\phi+2Z_1^2(\theta)\cos(\phi+120°)$ and $\epsilon=1$. The innermost solid and dashed contours are 0.4 and -0.4, respectively.

Bottom: $Z_1^1(\theta)\cos\phi+Z_1^2(\theta)\cos(\phi+90°)$ and $\epsilon=10$. The innermost solid and dashed contours are 0.6 and -0.6, respectively.

of the UV markings are undoubtedly the consequences of forced responses. In this case there is no single value of ϵ which suffices for the entire planet, as was true for free oscillations. Instead we must use the observed spatial structure and propagation speed of the markings to determine σ and s, and then refer to the dispersion relation to find the associated value of ϵ.

Once again we seek a combination of a first class oscillation with a second class oscillation shifted in phase by 90°. If a forced Rossby-Haurwitz wave with $s=1$ is to travel with a phase speed of about 15–20 m s^{-1}, ϵ must be between 5 and 10. For the purpose of illustration we use the latitudinal structure corresponding to $\epsilon=10$ [given by Longuet-Higgins (1968)]. The first class oscillation is now an internal gravity wave, and we have some flexibility in the choice of wave speed. We could again postulate a standing wave, which would make ϵ arbitrary, but let us interpret the data in the alternative way, namely, that the equatorial wave moves westward relative to the mean flow at a phase speed of 5–15 m s^{-1}.

We select the lowest symmetric latitudinal mode for each class, i.e., $n=1$ for the first class and $n=2$ for the second class. The first class mode is thus a Kelvin wave. Kelvin waves propagate only eastward on Earth, but in the retrograde rotating atmosphere of Venus they would propagate westward. For a Kelvin wave moving at 5 m s^{-1} on Venus, $\epsilon\approx1000$, while for one moving at 15 m s^{-1}, $\epsilon\approx500$.

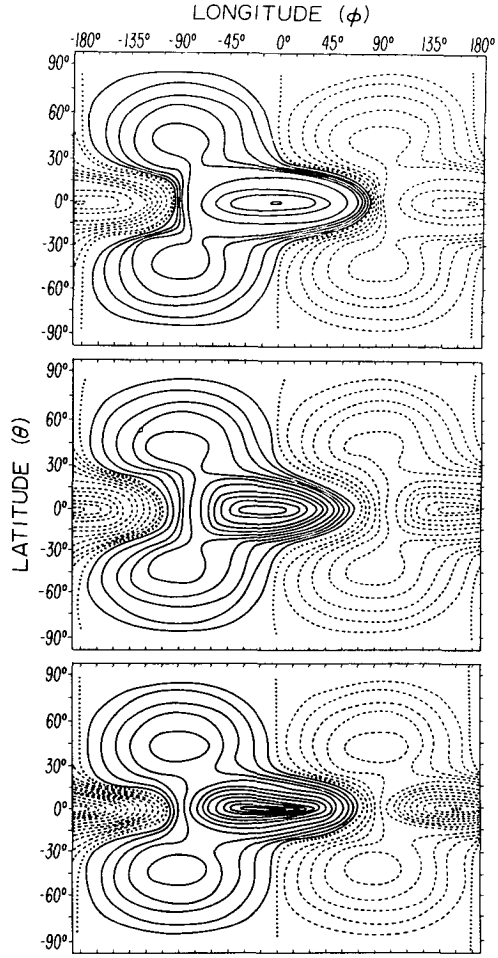

FIG. 22. Contours of surface elevation (pressure) for the forced oscillation case obtained by combining a Kelvin wave with a Rossby-Haurwitz wave shifted westward in phase relative to the Kelvin wave. The lowest symmetric latitudinal mode for each wave ($n=1, 2$, respectively) is shown. The zonal wavenumber is $s=1$. The latitudinal solutions are normalized so that the total energy over the sphere is a constant. The format is the same as in Fig. 22.

Top: $2Z_1^1(\theta)\cos\phi+Z_1^2(\theta)\cos(\phi+90°)$. $\epsilon=1000$ for Kelvin wave, $\epsilon=10$ for Rossby-Haurwitz wave. Dotted contour is 0.0. Contour interval is 0.1 between 0.0 and ±0.5 and 0.5 between ±0.5 and ±2.5.

Middle: $Z_1^1(\theta)\cos\phi+Z_1^2(\theta)\cos(\phi+90°)$. $\epsilon=500$–800 for Kelvin wave, $\epsilon=10$ for Rossby-Haurwitz wave. Dotted contour is 0.0. Contour interval is 0.1.

Bottom: $Z_1^1(\theta)\cos\phi+Z_1^2(\theta)\cos(\phi+90°)$. $\epsilon=1000$ for Kelvin wave, $\epsilon=10$ for Rossby-Haurwitz wave. Dotted contour is 0.0. Contour interval is 0.1.

The bottom of Fig. 22 shows the surface elevation or pressure fluctuation contours for the addition of the Rossby-Haurwitz ($\epsilon \approx 10$) and Kelvin ($\epsilon \approx 1000$) waves. There are some interesting differences from the case of free oscillations, although the overall structure of the lower amplitude contours is basically similar. In particular, if we consider the highest amplitude contours (≥ 0.5), we see that the Y breaks up into a distinct and extremely strong equatorial feature plus two separate lower amplitude regions at $\pm 45°$. This aspect of the pattern bears a striking resemblance to the observed structure of the UV markings. The tilt of the contour lines between 0° and $\pm 45°$ does not seem to agree quite as well with the observed tilt of the "cloud patterns" and the general Y morphology as does the tilt of the contours of the free oscillation pattern, but the forced oscillation pattern does reproduce the curvature in the two "arms" of the Y fairly well. The forced case gives a better representation of the longitudinal extent of the observed UV equatorial dark marking than does the free example.

For the purpose of comparison, we have plotted the contours for two other cases corresponding to a slight change of the parameters. The top of Fig. 22 shows the effect of doubling the amplitude of the Kelvin wave, with everything else kept constant, while the middle of the figure illustrates the pattern formed by using the value 12–15 m s^{-1} for the phase speed of the Kelvin wave (corresponding to $\epsilon \approx 500$–800). Longuet-Higgins (1968) has only provided latitudinal profiles for $\epsilon = 1$, 10, 10^2, 10^3, so we have visually estimated the profile for the case $\epsilon \approx 500$–800 from the structures of the profiles for $\epsilon = 10^2$ and $\epsilon = 10^3$. In both additional examples we see that the resulting pattern is basically the same, with two slight modifications. First, the equatorial and mid-latitudinal markings are now connected by a narrow region in the vicinity of $\pm 30°$, although the distinct nature of the features at 0° and $\pm 45°$ is still retained. Second, there is a more obvious tilt of the contours between the equator and mid-latitudes. There is perhaps slightly more of a tilt for the $\epsilon \approx 500$–800 case than for the doubled amplitude case.

These wave modes are not presented as a unique interpretation of the Mariner 10 data. We have only endeavored to show that these waves, which we expect to exist in Venus' atmosphere by analogy with Earth, can have associated pressure fluctuation patterns suggestive of the Y. A rigorous theory explaining this feature as a wave phenomenon would incorporate a model of forcing which selected the particular wave modes needed to construct the Y. The most important point to be made here is that the Y may be the manifestation of two or more wave phenomena occurring at different latitudes in such a way as to maintain their spatial relationship over a period of several days. Alternatively, it may be a single wave propagating in the nonuniformly rotating upper Venus atmosphere. Finally, although zonal wavenumber 1 represents the large-scale UV brightness variations during the 8 days of Mariner 10 observations there appears to be no reason why other zonal wavenumbers should not characterize the global UV contrasts at different times because of temporal variations in the forcing, for example. In addition, there do not appear to be any *a priori* reasons why the particular phase relationship we have chosen should always characterize the mix of planetary-scale waves described herein. Thus our explanation for the underlying physical cause of the morphology of the large-scale markings can easily accommodate the occasional appearance of wavenumber 2 or 3 in the pattern and also the modification of the Y pattern into the "inverted C" and "Psi" forms that have been reported (cf., Dollfus, 1975).

b. Circumequatorial belts

Although the nature of the circumequatorial belts cannot be definitively established from the Mariner 10 pictures alone, it seems reasonable to interpret them as waves, of the internal gravity type, propagating at the levels in the atmosphere characteristic of the UV clouds. These waves are generated dynamically or thermally and transport energy and momentum horizontally and vertically away from the region of excitation. The belts are either features of regional scale associated with the subsolar region or they are planetary or global in scale and visible in the UV only in the subsolar area because of the particular atmospheric conditions there. Assuming the phenomenon is of limited spatial extent, we compare the observations with properties of propagating plane waves.

Effects of rotation on such waves in the Venus atmosphere are small, even on the basis of the rotation rate of the 4-day circulation. The time scale or period associated with the motions of the CEB's is about 400 km (the horizontal wavelength) divided by 20 m s^{-1} (the horizontal phase velocity) or 2×10^4 s. This is an order of magnitude less than the 3.5×10^5 s period associated with the 4-day rotation. We note in addition that the Coriolis force is unimportant in modifying horizontal motions of the atmosphere in equatorial regions where the circumequatorial belts are observed.

To establish the plausibility of the gravity wave interpretation it is sufficient to consider the simplified theory of plane wave propagation in an isothermal, vertically stratified, static atmosphere. If there is a bulk velocity of the atmosphere, for example, the 4-day rotation, at the level in the atmosphere where the waves are propagating, we must of course consider the propagation relative to the mean flow. However, if the CEB's are wave *fronts*, their north to south propagation implies a horizontal phase velocity at right angles to the mean zonal motion and the wave propagation properties for the static case can be used directly.

Although the Venus atmosphere as a whole is not isothermal, sections of the lower stratosphere can be so considered; in any case, the essential properties of gravity wave propagation are described most simply and adequately for our purposes by the isothermal model.

The Väisälä frequency N is a high-frequency cutoff for internal gravity waves:

$$N^2=\frac{g}{H}-\frac{g^2}{c^2}. \tag{2}$$

The parameter H is the scale height of the isothermal atmosphere and c is the sound speed. For the upper Venus atmosphere we take $g=8.88\times10^2$ cm s^{-2}, $H=RT_0/g=5.3$ km ($T_0=250$ K and $R=1.89\times10^6$ cm^2 s^{-2} K^{-1}, the gas constant for CO_2), and $c=(\gamma RT_0)^{\frac{1}{2}}=2.57\times10^4$ cm s^{-1} ($\gamma=7/5$, the ratio of the specific heat at constant pressure to that at constant volume); N is then 2.2×10^{-2} rad s^{-1}. We have noted that the frequency associated with the motions of the circumequatorial belts is about $2\pi(2\times10^4\ \text{s})^{-1}=3.14\times10^{-4}$ rad s^{-1}, much less than the Väisälä frequency.

The dispersion relation for waves propagating in the isothermal atmosphere is

$$k_{\text{vertical}}^2=\frac{(N^2-\omega^2)}{V_{\text{horizontal}}^2}+\frac{\omega^2}{c^2}-\frac{1}{4H^2}, \tag{3}$$

where k_{vertical} is the vertical wavenumber $=2\pi/\lambda_{\text{vertical}}$, $\lambda_{\text{vertical}}$ is the vertical wavelength, and $V_{\text{horizontal}}$ is the horizontal phase speed. With $N=2.2\times10^{-2}$ rad s^{-1}, $V_{\text{horizontal}}=20$ m s^{-1}, $\omega=3.14\times10^{-4}$ rad s^{-1}, $c=2.57\times10^4$ cm s^{-1} and $H=5.3$ km, we find $\lambda_{\text{vertical}}=5.7$ km. The vertical wavelength is comparable to the local scale height and the phase velocity of the wave must be nearly vertical; the group velocity, on the other hand, is mainly horizontal. This vertical wavelength is a natural scale to expect for vertical motions, and it is large enough to prevent the difficulty which arises if the phase changes so rapidly with height that the waves cannot be resolved in the imagery. Since the upper Venus atmosphere is not in an isothermal state, we have used the value of the local scale height in the region of the atmosphere of interest as the constant scale height of our preceding estimate.

Because the CEB's appear as "cloud" features in the UV imagery, condensation and/or evaporation may be occurring, at least over part of the wave cycle, with the accompanying release or absorption of latent heat. Even if the UV "absorber" is not itself a condensible, the presence of other atmospheric constituents able to undergo phase changes or other reactions, e.g., the dehydration of an H_2SO_4 solution droplet, can influence the propagation of internal gravity waves. Latent heat production by gravity-wave-induced condensation may act as a self-generating mechanism which serves to maintain gravity wave propagation over the great horizontal distances observed both on Earth (Einaudi and Lalas, 1975) and Venus.

Lalas (1972) has studied the propagation of acoustic and internal gravity waves in a moist atmosphere; latent heat exchange decreases the horizontal phase speeds of internal gravity waves compared to those of a dry atmosphere. Thus, it may be necessary to associate a vertical wavelength somewhat larger than 5.7 km with the circumequatorial belts if they are indeed internal gravity waves.

It may also be possible to interpret the circumequatorial belts as gravity waves propagating along the top of a cloud deck or the interface of an inversion. Metcalf (1975) has reported the existence of horizontally propagating gravity waves trapped in a low-level inversion in the Earth's atmosphere.

For waves of long horizontal extent compared to their vertical scale, we would expect a dispersion relation of the form

$$\omega=k_{\text{horizontal}}\left[gH\left(\frac{\rho_2-\rho_1}{\rho_1+\rho_2}\right)\right]^{\frac{1}{2}}, \tag{4}$$

where ρ_1 and ρ_2 are the densities above and below the interface, respectively. Values of g, H and $k_{\text{horizontal}}$ have already been given. For a cloud composed of partially hydrated sulfuric acid mixed with CO_2 [specifically, a 76% H_2SO_4 solution with total abundances of H_2O and H_2SO_4 of 1.6×10^{-3} and 5.0×10^{-3}, respectively, by weight, as proposed by Young (1973)] and an overlying pure CO_2 atmosphere, we find that $(\rho_2-\rho_1)/(\rho_1+\rho_2)\approx3\times10^{-3}$ and gravity waves on the cloud top would propagate with horizontal phase speeds of ~13 m s^{-1}. If the cloud droplets are a 90% H_2SO_4 solution with weight abundances of 0.4×10^{-6} and 3.7×10^{-6} for H_2O and H_2SO_4, respectively (Wofsy and Sze, 1975), then a similar calculation gives wave speeds less than a meter per second. The Mariner 10 radio occultation temperature profile (Howard *et al.*, 1974) shows a strong inversion at ~62 km altitude; from this we estimate an associated density change $(\rho_2-\rho_1)/(\rho_2+\rho_1)$ of ~0.005 and a horizontal phase velocity for waves on this interface of ~16 m s^{-1}. The above velocities are similar to observed speeds of CEB's.

We are still faced with explaining why the belts are found only near the equator and the subsolar region and why they appear to propagate only southward. These characteristics may be related to the mechanism of generation and propagation of the waves or to special atmospheric conditions near the subsolar region which make the waves visible only there. For example, if the CEB's are interface waves on an inversion, they may have been seen near the subsolar region because that is where the inversion was located. However, we have no knowledge of thermal profiles in other locations at the time of Mariner 10.

Effects of rotation on gravity wave propagation may influence the visibility of CEB's. Due to the addition of a Coriolis term to the dispersion relation gravity waves of different wavelengths will not travel at the same speed. However, Coriolis effects are unimportant at the equator, so a wave which is dispersive in mid-latitudes will not be dispersive near the equator. We might then picture a mechanism which excites several different wavelengths. In mid-latitudes these would travel at different speeds, destructively interfering with each other and thereby preventing their resolution in the UV imagery. As the waves approached the equator, they would all tend toward the same phase speed. There would be no destructive interference, and this might render them visible. Thus, even though rotational effects are expected to be unimportant dynamically, they could have an indirect influence on observations of the waves.

Understanding the southward propagation of the waves may require identification of the source mechanism. Internal gravity waves can carry energy and momentum upward to regions of lower density as well as horizontally. Thus, internal gravity waves tend to increase in amplitude with height. The features we observe in the lower stratosphere of Venus may only be manifestations of small oscillations generated much deeper in the atmosphere. On the other hand, if they are gravity waves propagating along an interface, they are most likely generated at or near the level of the discontinuity. At present we cannot choose between these two modes of propagation and generation. It is interesting that gravity waves so far observed in satellite imagery of the Earth's atmosphere propagate essentially southward and eastward (Thomas *et al.*, 1975).

Gravity waves in the Earth's atmosphere are known to be generated by the passage of weather systems, substorm activity in the upper atmosphere, instabilities in the general circulation, earthquakes and explosions, but the identification of the source of the circumequatorial belts is presently speculative. The association of the belts with the subsolar region and their occurrence just prior to the appearance of the bow-like waves suggest that the CEB's are generated by intense solar heating and convection, possibly at lower levels of the atmosphere, and that the waves carry heat away from regions of most intense heat deposition.

c. Cellular features

Cellular patterns are associated with thermal convection in laboratory fluids, in the Earth's atmosphere, and in the outer regions of the Sun. It seems unavoidable that the cellular structures in the subsolar region of the upper Venus atmosphere are associated with thermal convection there.

The widespread existence of two types of mesoscale cellular convection patterns in the atmospheres of both Earth and Venus invites the speculation that a similar physical phenomenon is involved in both cases. Properties of "open" and "closed" cells that exist beneath low-lying maritime inversions have been reviewed by Agee *et al.* (1973) and further analyzed by Krishnamurti (1975a, b, c). The distinction between the two types of cells, both of which have hexagonal patterns, is the direction of circulation. "Open" cells have descending motions at their centers which are clear of clouds; the reverse is the case for "closed" cells. The existence of the cells over wide areas of the Pacific and Atlantic Oceans is largely due to the presence of the low-level trade wind inversion which restricts the vertical scale of the convection, and thus the Rayleigh number of the flow, thereby providing suitable conditions for the formation of a cellular pattern rather than the more ubiquitous roll pattern. The major property of the terrestrial cells that concerns us here is that their diameter-to-depth ratios differ by roughly a factor of 2, with closed cells being characterized by a ratio of 30:1 and open cells by a ratio of 15:1. A further property is that they exist only in regions with small vertical wind shear.

The reason(s) for the large diameter-to-depth ratios (relative to laboratory and theoretical experience) is not fully understood (cf. Krishnamurti, 1975c). However, such large values seem to be a common property of geophysical systems, e.g., convection in large ponds (Woodcock and Riley, 1947). We will assume that the terrestrial ratios for open and closed cells apply to Venus. With this assumption and the association of bright-rimmed Venusian cells with the open variety and dark-bounded cells with the closed ones, we find that both types of Venusian cells imply a depth for the convecting region of about 15 km. This, perhaps fortuitously, is essentially the vertical extent of the region immediately below the 60 km level in the radio occultation temperature profiles that is close to the dry adiabat for CO_2.

On the basis of this analogy with terrestrial convection, we can make the following statements about conditions between $\sim$50 and 60 km in the Venus atmosphere:

1) The wind shear is probably no more than 2 or 3 m s^{-1} km^{-1}, the terrestrial value (Agee and Dowell, 1974).

2) The Rayleigh number, based on an eddy viscosity, is of the order of the terrestrial value, 5×10^4, or less (Krishnamurti, 1975c).

Statement 1) does not seem to be in conflict with what we know about the vertical shear in the Venusian zonal wind (Marov *et al.*, 1973; Ainsworth and Herman, 1975). Statement 2) has implications for the eddy diffusivity in the Venus atmosphere, according to the following.

The Rayleigh number R is

$$R = \frac{g\alpha d^4}{\nu\kappa}\frac{d\theta}{dz}, \quad (5)$$

where α is the coefficient of thermal expansion, d the thickness of the convecting region, ν the eddy viscosity, κ the eddy thermal diffusivity, and $d\theta/dz$ the vertical gradient of potential temperature. If we assume that $d\theta/dz$ is the same for this convecting layer of the Venus atmosphere as it is for mesoscale convective regions on Earth [$\sim 1°C\ km^{-1}$ (Krishnamurti, 1975c)], and recall that $\alpha \approx 1/T$, then we can determine the product $\nu\kappa$ from (5) and parameter values already specified. If we also take $\nu \approx \kappa$, then a very large eddy viscosity, $\nu \gtrsim 5\times 10^7\ cm^2\ s^{-1}$, is implied. We note that just above the convective layer, in a region several kilometers higher than the visible cloud deck, the eddy viscosity is probably $10^4-10^5\ cm^2\ s^{-1}$, based on photochemical arguments of McElroy *et al.* (1973) and Prinn (1975). Since this region is stable, the higher eddy viscosity we infer for the unstable convective layer at lower altitude is not unreasonable.

d. Bow-like waves

Bow-like waves may be the consequence of an interaction between the zonal circulation of the upper atmosphere and the subsolar disturbance, which provides a possible pressure or temperature "obstacle" to the fast atmospheric rotation. Internal gravity waves, generated in the interaction, may coalesce nonlinearly to form the bow-like waves, in a manner similar to the generation of upstream bow shocks in "supercritical" flows past obstacles. Such an explanation seems possible, since an entire spectrum of internal gravity waves with horizontal phase speeds less than the 100 m s^{-1} upstream wind velocity could be produced in the interaction. In fact, it is unlikely that internal gravity waves with horizontal phase velocities larger than 100 m s^{-1} would be generated; Eq. (3) would imply a vertical wavelength larger than 25 km for waves moving faster than 100 m s^{-1} horizontally.

If the above explanation is correct, we must question why the observed bow-like wave is not a steady feature of the interaction and why, once formed, it drifts downstream essentially with the speed of the atmospheric circulation. One possibility is that the temperature and/or pressure amplitudes in the underlying bow-like wave are not always appropriate to produce any visual (i.e., UV) evidence of its presence, but that on transitory occasions the amplitudes can grow sufficiently to produce a UV "marker." Once the structure is revealed its signature is then advected downstream by the flow in much the same way as a dye would be in a laboratory experiment. If this conjecture is correct then it is possible that in the observed bow-like waves we may be seeing the visible manifestation of one of the major processes which act to limit the magnitude of the zonal flow.

6. Summary

We have given detailed descriptions and interpretations of phenomena seen in the UV markings on Venus during the Mariner 10 encounter of the planet. The large-scale brightness distribution appears to be most simply described in terms of a pattern with zonal wavenumber 1 which extends between about $\pm 50°$ latitude and which progresses around the planet in about 4.2 days. With increasing latitude, the phase of the brightness variations advances westward, in the direction of rotation of the pattern. The feature is essentially symmetrical about the equator and maintains its global morphology over the approximately two rotations of the structure observed by Mariner 10. The overall effect is to produce the impression of a diffuse, horizontal Y similar in form to that reported by ground-based observers.

Because of the global coherence of the large-scale brightness variations and because the pattern moves with respect to the actual zonal winds in the atmosphere, as seems to be indicated by tracking small-scale UV features, we have interpreted the large-scale UV markings as a wave phenomenon. We have shown how the observed Y pattern can be produced, for example, by the superposition of two planetary scale waves, a Rossby-Haurwitz wave dominant at mid-latitudes and a Kelvin wave dominant near the equator. We have not claimed that this particular set of waves is necessarily responsible for the large-scale UV brightness variations on Venus; we have only noted the feasibility and plausibility of the identification.

A quantitative description of the circumequatorial belts and bow-like waves was given. The genesis of both phenomena is closely related to processes occurring near the subsolar point. The belts, which are observed only between $\pm 20°$ latitude, are essentially parallel to latitude circles and propagate southward at speeds of about 20 m s^{-1}. They have a wavelength of about 500 km and a zonal extent of up to 5000 km. We believe the belts to also be a wave phenomenon, albeit on a regional scale. Possibilities include internal gravity waves (perhaps modified by condensation) with vertical wavelength comparable to a local scale height and gravity waves propagating along an effective density discontinuity, e.g., a hypothetical cloud top or a sharp temperature inversion.

The bow-like waves propagate zonally at 93 ± 5 m s^{-1} and are formed a few degrees upwind of the subsolar point. We proposed that the bow-like waves may be true bow waves formed by the interaction of the rapid, supercritical zonal flow with internal gravity waves of lower horizontal phase speeds generated by the subsolar disturbance.

Markings near the subsolar point are often chaotic and difficult to follow between successive frames. However, two types of cellular features observed in equatorial regions can be mapped and described. One consists of bright-rimmed cells with darker centers; the others are bright-centered structures bounded by a dark filamentary network. The horizontal, linear scale of dark-bounded features is approximately twice that of bright-rimmed cells. Our interpretation of these features is based on an analogy with mesoscale convection cells seen in the Earth's maritime atmosphere. This analogy implies that convection is occurring near the subsolar region through a layer about 15 km deep, and that downdrafts are associated with regions of darker UV markings.

The UV markings in mid-latitudes are characterized by a high degree of organization on all length scales. The finestructure is composed of bright and dark parallel "spiral streaks" of width $\sim$100 km and length $\sim$1000 km. On a global scale these form the basis of a system of much larger bright "spiral bands" in both the Northern and Southern Hemispheres. The inclination of these bands to lines of latitude appears to be linked to the brightness of material covering the equator.

Detailed observations of the southern polar ring show that it is a feature whose position and intensity at a given longitude with respect to the subsolar point are variable in time. The "ring" is not always parallel to latitude circles and even a break in the structure is evident in one of the images. Only in the south polar region are UV contrasts also visible in the orange.

7. Concluding remarks

In this paper we have tried to provide more complete and quantitative descriptions than hitherto available of the forms and motions of the UV markings in Mariner 10 pictures. We have also attempted to provide reasonable interpretations of the phenomena in the Venus upper atmosphere revealed by these markings. If our guesses are correct, then the upper Venus atmosphere is a most intriguing place; waves of planetary and regional scale are propagating relative to the rapidly rotating atmospheric circulation and thermal convection in the subsolar region creates a complex interaction with the fast-moving winds. The unique circulatory regime of the Venusian atmosphere challenges our understanding of atmospheric dynamics; we can learn a great deal relevant to our own atmosphere by understanding the processes occurring on Venus. Our present understanding of Venus' atmospheric dynamics is severely limited by lack of data, a situation that Pioneer Venus, with its entry probes and year-long orbital reconnaissance of the planet, will do much to correct.

Acknowledgments. We gratefully acknowledge the enthusiastic cooperation of J. Soha, D. Elliott and R. Dewar of the Image Processing Laboratory of the Jet Propulsion Laboratory (JPL) in the preparation of the picture material and also the generous assistance of K. Klaasen in his role as the JPL experiment representative to the Mariner 10 TV team. G. Schubert and A. Del Genio were supported by NASA under NSG 7164.

REFERENCES

Agee, E. M., T. S. Chen and K. E. Dowell, 1973: A review of mesoscale cellular convection. *Bull. Amer. Meteor. Soc.*, **54**, 1004–1012.

——, and K. E. Dowell, 1974: Observational studies of mesoscale cellular convection. *J. Appl. Meteor.*, **13**, 46–53.

Ainsworth, J. E., and J. R. Herman, 1975: Venus wind and temperature structure: The Venera 8 data. *J. Geophys. Res.*, **80**, 173–179.

Beebe, R. F., 1972: Ultraviolet clouds on Venus: Observational bias. *Icarus*, **17**, 602–607.

Belton, M. J. S., G. R. Smith, D. A. Elliott, K. Klaasen and G. E. Danielson, 1976: Space-time relationships in the UV markings on Venus. *J. Atmos. Sci.*, **33**, 1383–1393.

Boyer, C., and P. Guérin, 1969: Étude de la rotation rétrograde, en 4 jours, de la couche extérieure nuageuse de Vénus. *Icarus*, **11**, 338–355.

Chang, C.-P., 1970: Westward propagating cloud patterns in the tropical Pacific as seen from time-composite satellite photographs. *J. Atmos. Sci.*, **27**, 133–138.

Dollfus, A., 1975: Venus: Evolution of the upper atmospheric clouds. *J. Atmos. Sci.*, **32**, 1060–1070.

Dunne, J. A., 1974: Mariner 10 Venus encounter. *Science*, **183**, 1289–1291.

Einaudi, F., and D. P. Lalas, 1975: Wave-induced instabilities in an atmosphere near saturation. *J. Atmos. Sci.*, **32**, 536–547.

Fels, S. B., and R. S. Lindzen, 1974: The interaction of thermally excited gravity waves with mean flows. *Geophys. Fluid Dyn.*, **6**, 149–191.

Hansen, J. E., and J. W. Hovenier, 1974: Interpretation of the polarization of Venus. *J. Atmos. Sci.*, **31**, 1137–1160.

Hines, C. O., 1972: Gravity waves in the atmosphere. *Nature*, **239**, 73–78.

Holton, J. R., 1972: *An Introduction to Dynamic Meteorology*. Academic Press, 278–295.

Howard, H. T., G. L. Tyler, G. Fjeldbo, A. J. Kliore, G. S. Levy, D. L. Brunn, R. Dickinson, R. C. Edelson, W. L. Martin, R. B. Postal, B. Seidel, T. T. Sesplaukis, D. L. Shirley, C. T. Stelzried, D. N. Sweetnam, A. I. Zygielbaum, P. B. Esposito, J. D. Anderson, I. I. Shapiro, and R. D. Reasenberg, 1974: Venus: Mass, gravity field, atmosphere, and ionosphere as measured by the Mariner 10 dual-frequency radio system. *Science*, **183**, 1297–1301.

Krishnamurti, R., 1975a: On cellular cloud patterns. Part 1: Mathematical model. *J. Atmos. Sci.*, **32**, 1353–1363.

——, 1975b: On cellular cloud patterns. Part 2: Laboratory model. *J. Atmos. Sci.*, **32**, 1364–1372.

——, 1975c: On cellular cloud patterns. Part 3: Applicability of the mathematical and laboratory models. *J. Atmos. Sci.*, **32**, 1373–1383.

Lacis, A. A., 1975: Cloud structure and heating rates in the atmosphere of Venus. *J. Atmos. Sci.*, **32**, 1107–1124.

Lalas, D. P., 1972: Effect of moisture on the propagation of internal and acoustic gravity waves. *Phys. Fluids*, **15**, 734–736.

Leovy, C. B., 1973: Rotation of the upper atmosphere of Venus. *J. Atmos. Sci.*, **30**, 1218–1220.

Longuet-Higgins, M. S., 1968: The eigenfunctions of Laplace's tidal equations over a sphere. *Phil. Trans. Roy. Soc. London*, **A262**, 511–607.

Marov, M. Ya., V. S. Avduevsky, V. V. Kerzhanovich, M. K. Rozhdestvensky, N. F. Borodin and O. L. Ryabov, 1973:

Venera 8: Measurements of temperature, pressure, and wind velocity on the illuminated side of Venus. *J. Atmos. Sci.*, **30**, 1210–1214.

McElroy, M. B., N. D. Sze and Y. L. Yung, 1973: Photochemistry of the Venus atmosphere. *J. Atmos. Sci.*, **30**, 1437–1447.

Metcalf, J. I., 1975: Gravity waves in a low-level inversion. *J. Atmos. Sci.*, **32**, 351–361.

Murray, B. C., M. J. S. Belton, G. E. Danielson, M. E. Davies, D. Gault, B. Hapke, B. O'Leary, R. G. Strom, V. Suomi and N. Trask, 1974: Venus: Atmospheric motion and structure from Mariner 10 pictures. *Science*, **183**, 1307–1315.

Prinn, R. G., 1975: Venus: Chemical and dynamical processes in the stratosphere and mesosphere. *J. Atmos. Sci.*, **32**, 1237–1247.

Ramanathan, V., and R. D. Cess, 1975: An analysis of the strong zonal circulation within the stratosphere of Venus. *Icarus*, **25**, 89–103.

Schubert, G., and R. E. Young, 1970: The 4-day Venus circulation driven by periodic thermal forcing. *J. Atmos. Sci.*, **27**, 523–528.

Scott, A. H., and E. J. Reese, 1972: Venus: Atmospheric rotation. *Icarus*, **17**, 589–601.

Suomi, V., 1974: Cloud motions on Venus. *The Atmosphere of Venus*, J. Hansen, Ed. Goddard Institute for Space Studies, NASA SP-382, 42–58.

Taylor, G. I., 1936: The oscillations of the atmosphere. *Proc. Roy. Soc. London*, **A156**, 318–326.

Thomas, J. E., M. D. Kays, J. D. Horn and R. L. Moore, 1975: Visual observation of propagating gravity waves on ATS III satellite film loops. Tech. Rept. ECOM-5553. U. S. Army Electronics Command.

Traub, W. A., and N. P. Carleton, 1975: Spectroscopic observations of winds on Venus. *J. Atmos. Sci.*, **32**, 1045–1059.

Wallace, J. M., 1973: General circulation of the tropical lower stratosphere. *Rev. Geophys. Space Phys.*, **11**, 191–222.

Witt, G., 1962: Height, structure, and displacements of noctilucent clouds. *Tellus*, **14**, 1–18.

Wofsy, S. C., and N. D. Sze, 1975: Venus cloud models. *Atmospheres of Earth and the Planets*, B. M. McCormac, Ed., D. Reidel, 369–384.

Woo, R., 1975: Observations of turbulence in the atmosphere of Venus using Mariner 10 radio occultation measurements. *J. Atmos. Sci.*, **32**, 1084–1090.

Woodcock, A. H., and G. A. Riley, 1947: Patterns in pond ice. *J. Meteor.* **4**, 100–101.

Young, A. T., 1973: Are the clouds of Venus sulfuric acid? *Icarus*, **18**, 564–582.

——, 1975a: Is the four-day "rotation" of Venus illusory? *Icarus*, **24**, 1–10.

——, 1975b: The clouds of Venus. *J. Atmos. Sci.*, **32**, 1125–1132.